Remote Sensing of Environment 213 (2018) 34–48

Contents lists available at ScienceDirect

Remote Sensing of Environment

journal homepage: www.elsevier.com/locate/rse

Grassland canopy cover and aboveground biomass in Mongolia and Inner Mongolia: Spatiotemporal estimates and controlling factors

Ranjeet John[a,*], Jiquan Chen[a], Vincenzo Giannico[a,b], Hogeun Park[a], Jingfeng Xiao[c], Gabriela Shirkey[a], Zutao Ouyang[a], Changliang Shao[d], Raffaele Lafortezza[a,b], Jiaguo Qi[a]

[a] Center for Global Change and Earth Observations, Michigan State University, MI 48823, USA
[b] The Department of Agricultural and Environmental Science, The University of Bari Aldo Moro, Via Amendola 165/A, 70126 Bari, Italy
[c] Earth Systems Research Center, Institute for the Study of Earth, Oceans, and Space, University of New Hampshire, Durham, NH 03824, USA
[d] Institute of Agricultural Resources and Regional Planning, Chinese Academy of Agricultural Sciences, Beijing 100081, China

ARTICLE INFO

Keywords:
Grasslands
Semiarid
MODIS
Cubist
Livestock density
Mongolian Plateau

ABSTRACT

Temperate and semiarid grasslands comprise 80% of the land area on the Mongolian Plateau and environs, which includes Mongolia (MG), and the province of Inner Mongolia (IM), China. Substantial land cover/use change in the last few decades, driven by a combination of post-liberalization socioeconomic changes and extreme climatic events, has degraded these water-limited grassland's structure and function. Hence, a precise estimation of canopy cover (CC, %) and aboveground biomass (AGB, g m^{-2}) is needed. In this study, we analyzed > 1000 field observations with sampling during June, July and August (JJA) in 2006, 2007, 2010 and 2016 in IM and 2010–2012 and 2014–2016 in MG. The field sampling was stratified by the dominant vegetation types on the plateau, including the meadow steppe, the typical steppe, and the desert steppe. Here we used Moderate Resolution Imaging Spectroradiometer (MODIS) derived surface reflectance and vegetation indices optimized for low cover conditions to develop and test predictive models of CC and AGB using observed samples as training and validation data through rule-based regression tree models. We then used the predictive models to estimate spatially-explicit CC and AGB for the plateau over the last decade (2000–2016). Our study demonstrated the effectiveness of our predictive models in up-scaling ground observations to the regional scale across steppe types. Our results showed that model R^2 and RMSE for CC and AGB were 0.74 (13.1%) and 0.62 (85.9 g m^{-2}), respectively. The validation R^2 and RMSE for CC and AGB were 0.67 (14.4%) and 0.68 (76.9 g m^{-2}), respectively. The mean ± SD for CC and AGB were 24.9 ± 23.4% and 155.2 ± 115.2 g m^{-2}, respectively. We also found that our scaled up estimates were significantly related to inter-annual climatic variability and anthropogenic drivers especially distance to urban/built-up areas and livestock density. In addition to their direct use in quantifying the spatiotemporal changes in the terrestrial carbon budget, results from these predictive models can help decision makers and rangeland managers plan sustainable livestock practices in the future.

1. Introduction

Semiarid ecosystems cover 41% of the terrestrial surface and support 38% of the global population, of which a greater proportion includes most developing countries (Reynolds et al., 2007). While tropical forest biomes dominate the terrestrial carbon sink, its inter-annual variability is controlled by semiarid ecosystems which are strongly associated with circulation-driven variations in precipitation and temperature (Ahlström et al., 2015). Higher carbon turnover rates in semiarid ecosystems were found to be important drivers of inter-annual variability of the global carbon cycle with projections suggesting that tropical forest ecosystems might become less relevant drivers (Poulter et al., 2014). The canopy cover (CC) and above ground biomass (AGB) of these semiarid ecosystems are relatively low, but given their large extent, climate driven dynamics coupled with anthropogenic modification can significantly impact their vegetation structure and function as well as regional and global carbon budgets (Ahlström et al., 2015).

The Eurasian steppe constitutes a major portion of global temperate grasslands and forms a contiguous belt across the continent from the Mediterranean basin to eastern China (Wesche et al., 2016; Qi et al., 2017). The Mongolian steppe represents a significant proportion of the

* Corresponding author.
E-mail address: ranjeetj@msu.edu (R. John).

https://doi.org/10.1016/j.rse.2018.05.002
Received 14 July 2017; Received in revised form 28 April 2018; Accepted 1 May 2018

Eurasian steppe that is largely intact with high biodiversity (John et al., 2008; Khishigbayar et al., 2015). However, these grasslands and the pastoralists that they support face an uncertain future owing to interactions among a warming trend over the past 50 years, an increasing frequency in extreme climate events, rapid changes in land cover/use (e.g., increasing grazing density and mining) and changes in governance and policies (Fernández-Giménez et al., 2012; Reid et al., 2014; Chen et al., 2015b; Khishigbayar et al., 2015; John et al., 2016; Fernández-Giménez et al., 2017). Precipitation, the major limiting factor in these semiarid ecosystems, has high temporal and spatial variability, while a combination of droughts and *dzuds* (i.e., severe winter associated with high livestock mortality) is known to explain the inter-annual dynamics in AGB (Bai et al., 2004; John et al., 2013b).

Livestock sustainability in Mongolia and other semiarid ecosystems depends on dry season forage which has high spatiotemporal variability (Jacques et al., 2014). The timely monitoring of CC and AGB through synoptic-scale remote sensing is thus essential for forage estimation and in turn, determination of carrying capacity of livestock population enabling regulation of stocking rates for sustainable use of grassland resources (Rasmussen et al., 1999; Marsett et al., 2006). The impact of both climate and anthropogenic drivers on ecosystem structure and function as represented by CC and AGB is of significance to our understanding of carbon stocks of the Mongolian Plateau (MP)'s grassland ecosystems (Xie et al., 2009; Zhang et al., 2014).

Scientific investigations on estimating CC and AGB in semiarid environments over large extents (e.g. the Sahel and the MP) recommend sampling data over a range of vegetation types, biomes and vegetation zones over the growing season in order to obtain robust calibration models (Guan et al., 2012; Jacques et al., 2014; Ferner et al., 2015). Most grassland scale-up studies are limited in terms of measurements (Ma et al., 2010) or sampling extent along relatively short environmental gradients. Furthermore, very few studies cover different phenological stages of the growing season (Jacques et al., 2014; Ferner et al., 2015). Such surveys are both expensive and time-consuming and, therefore, satellite-based remote sensing using wide-swath sensors like the MODerate-resolution Imaging Spectroradiometer (*MODIS*) are especially valuable in remote areas of large areal extent like the MP for rapid acquisition of vegetation seasonal dynamics at the landscape and regional scales. Satellite-derived vegetation indices (VI) are considered as proxies of primary productivity and linearly related to several biophysical variables such as canopy cover (i.e., the proportion of surface unit area obscured by vegetation matter when viewed from above), leaf area, and chlorophyll (Tucker and Sellers, 1986). VIs from Landsat TM or MODIS obtained during the same month and year (Xie et al., 2009; Zhao et al., 2014) have been used to scale-up CC and AGB from the landscape to the regional scale through statistical models (Halperin et al., 2016; Zhang et al., 2016). However, these empirical models have serious drawbacks owing to uncertainties in their model coefficients which are site-specific and differ by ecosystem type and season. In addition, most CC and AGB scale-up models are based on the normalized difference vegetation index (NDVI), which is sensitive to the soil background signature and therefore not optimal for semiarid ecosystems with < 50% canopy cover (Huete et al., 2002; Chopping et al., 2008; Jacques et al., 2014). There have been few studies which focused on large area estimation of dry forage and canopy cover using dry vegetation VIs optimized for low cover conditions (e.g., enhanced vegetation index (EVI), normalized difference senescence vegetation index (NDSVI) (Marsett et al., 2006; Chopping et al., 2008; Jacques et al., 2014; Guerschman et al., 2015). The ability of MODIS-derived dry forage indices to estimate dry season biomass has also been limited due to the lack of representative, in situ data to serve as training data.

Non-parametric, data-mining/machine learning methods (e.g., Random Forest and Cubist) have been used in the recent past to scale-up net ecosystem production (NEP) and gross primary production (GPP) from eddy covariance towers (Xiao et al., 2010; Wylie et al., 2016). However, few studies have used RF or Cubist to scale-up from extensive, in situ samples of CC (Lehnert et al., 2015; Halperin et al., 2016) and fewer still for AGB scale-up (Blackard et al., 2008) to the national scale. Regression tree algorithms, and Cubist in particular are uniquely suited for dealing with nonlinear relationships, utilizing continuous and categorical variables, and modeling complex interactions (Xiao et al., 2010; Wylie et al., 2016). They also provide an alternative to precipitation driven, process based models which are limited by the spatial variability of rainfall and by the sparseness of meteorological stations in remote areas such as the Eurasian Steppe (Wylie et al., 2016). While regression trees are prone to overfitting, this drawback can be attenuated through cross validation and combining several rule-based models into committee models which are averaged for a final prediction (Xiao et al., 2008; Wylie et al., 2016).

Most scale-up studies on the MP are limited by extent as it is difficult to obtain in situ measurements while maintaining an adequate number for stratified random sampling (Feng et al., 2005; Gao et al., 2012; Zhao et al., 2014). A notable exception is a study where net ecosystem production was scaled up from eddy covariance flux towers and MODIS VIs in Inner Mongolia and surrounding provinces to obtain regional coverage using Cubist rule-based models (Zhang et al., 2014). There have been far fewer scaling up studies in Mongolia, which are limited temporally and in spatial extent (Angerer, 2012). Thus, there exists a knowledge gap regarding CC and AGB estimates that can be addressed by developing remote sensing products customized for the MP.

Here we investigate the relationships between extensive in situ measurements across the MP and VIs derived from the MODIS *Nadir BRDF Adjusted Reflectance* (*NBAR*) product using regression tree rule-based models. Our objectives were to: 1) develop non-parametric predictive models to scale-up CC and AGB using MODIS 500 m data along with ancillary variables across the entire MP; 2) model uncertainties and quantify inter-annual variability of peak season CC and AGB; and 3) explain the spatiotemporal heterogeneity of CC and AGB by examining the impact of anthropogenic drivers and inter-annual climatic variability.

2. Materials and methods

2.1. Study area

The MP covers approximately 2.7×10^6 km, bounded by 35°N -55°N latitude and 90°E-130°E longitude. The elevation of the MP varies greatly with an average elevation of over 1285 m and a relief of 4198 m. Mean annual temperature ranges from −4.5 °C to 8.6 °C (Yu et al., 2003; Nandintsetseg et al., 2007; Bai et al., 2008), while the mean annual precipitation (MAP) varies from 368 mm in the meadow steppe to 166 mm in the desert steppe, with up to 75% of annual rainfall occurring during the summer (JJA) (Rao et al., 2015). The plateau includes three steppe types, the meadow-mountain steppe, the typical steppe, and the desert steppe (25.1, 26.1 and 27.2% of the entire area, respectively) (Hilker et al., 2014; Wesche et al., 2016), with their distribution determined mostly by the precipitation gradient (Fig. 1). The typical steppe corresponds to the cold, semi-arid climate type (BSk) of the Köppen classification with a MAP of 300 mm. The typical steppe is predominantly herbaceous in nature with a vegetation cover of 25–100% that is characterized by *Stipa krylovii, Stipa grandis*, *Carex duriusula, Cleistogenes spp.*, *Leymus Chinenis*, and *Artemisia frigida* (in overgrazed areas). The meadow-mountain Steppe corresponds to the subarctic climate in the northeast with cool summers and severe dry winters (Dwc) in the Khangaii Mountains of Mongolia and the Greater Khingan Mountains in Inner Mongolia with a MAP of 400 mm. The meadow steppe consists of moist grasslands with high canopy cover of 60–90% (Liu et al., 2013), and herbaceous species that are less tolerant to drought, including species such as *Poa attenuata*, *Festucca lenensis*, *Stipa baicalensis*, *Filifolium sibiricum*, *Leymus Chinenis*, *Carex pediformis* and *Artemisia frigida* (Fernández-Giménez and Allen-Diaz, 1999; Khishigbayar et al., 2015). The desert steppe corresponds to the cold

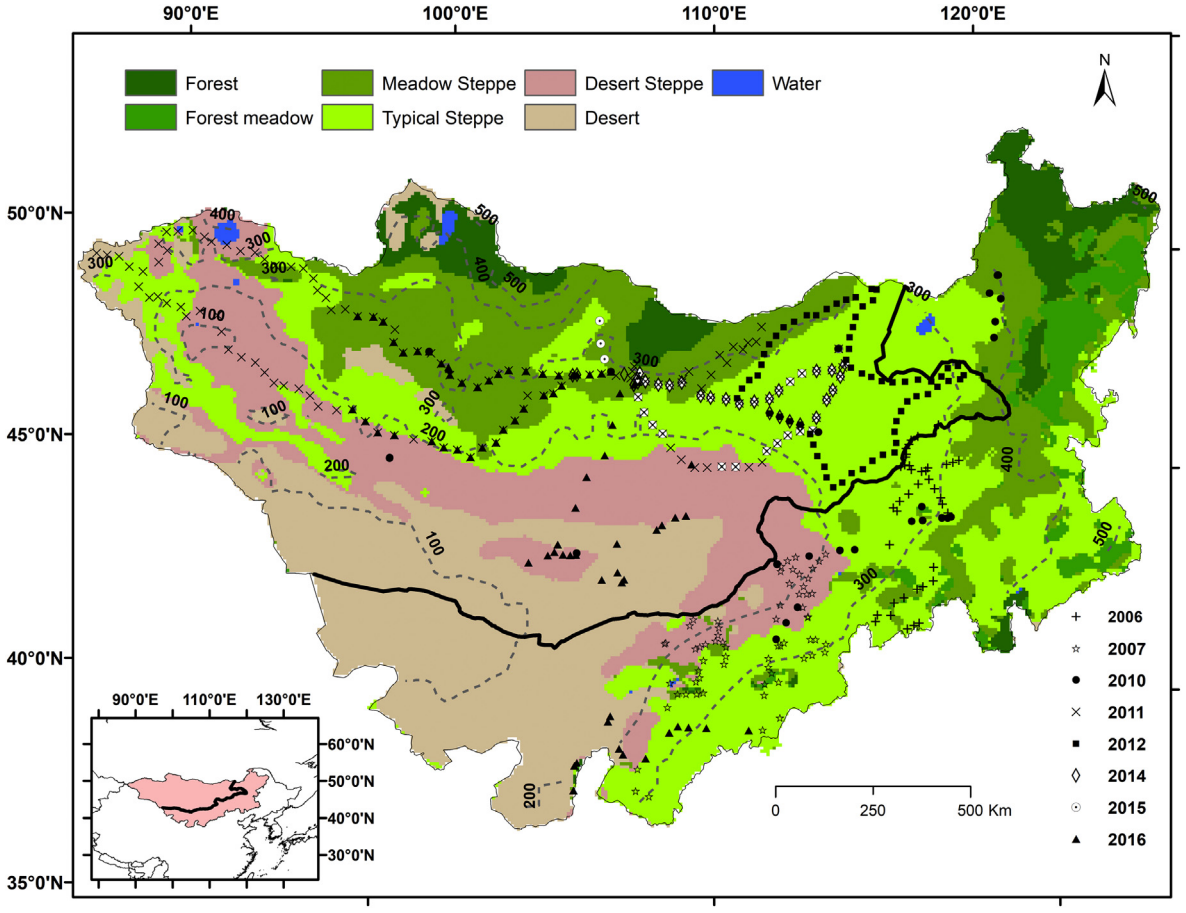

Fig. 1. Multi-year in situ measurements and isohyets (dashed lines) derived from CRU TS323 mean annual precipitation (1981–2014) overlaid on vegetation types on the Mongolian Plateau and its environs. The thick line denotes the border between the Republic of Mongolia and the province of Inner Mongolia, China.

desert climate of BWk with a MAP of 150–200 mm. The desert steppe has more open vegetative cover (10–25%) and is characterized by xerophytic shrubs such as *Caragana spp.*, *Artemisa xerophytica,* and *Artemisia ordosica,* perennial forbs such as *Allium polyrrhizum and Allium anisopodium,* and xerophyte herbs like *Stipa gobica* (John et al., 2013a; Liu et al., 2013; John et al., 2016; Wesche et al., 2016).

2.2. Field measurements and sampling design

We sampled across diverse precipitation and grazing pressure gradients in the dominant steppe types on the MP (Fig. 1). Field sampling was carried out over a period of 10 years (2006–2016) with a total of 1188 sampling sites. The measurements were sampled extensively over different phenological stages during JJA and were also well distributed over MAP regimes (150–500 mm). Each sampling site is representative of the dominant steppe vegetation type for that particular landscape and is relatively homogeneous (Table 1). We used the conventional plot-based quadrats technique that have been widely applied in community ecology of grassland studies for estimating canopy cover. Specifically we used a 0.5 × 0.5 m quadrat with three replicates within a 30 × 30 m plot at each site. CC, AGB, and species were recorded at each quadrat. Prior to each field season, the quadrat frame was marked by 10 × 10 grid mesh to assure CC estimate accuracy and consistency. CC was measured by counting grid squares filled with vegetation. The AGB of herbaceous grassland species was measured by harvesting herbaceous samples clipped at the ground level and their green (or wet) weight noted using a field balance. Samples were oven dried later at the laboratory and then weighed.

Our sampling sites also covered different levels of grazing pressure

Table 1
The mean (SD) of in situ canopy cover (CC) (%) and aboveground biomass (AGB) ($g\,m^{-2}$) of different steppe types on the Mongolian Plateau, between June and August during 2006–2016 (n = 1187).

Year	Type	n	CC (%)		AGB ($g\,m^{-2}$)	
2006	Meadow Steppe	2	57.5	(14.2)	349.4	(199.8)
	Typical Steppe	38	42.9	(19.5)	207.9	(147.8)
2007	Forest Steppe	2	29.2	(0.8)	204.6	(36.6)
	Meadow Steppe	6	37.5	(20.6)	428.9	(283.7)
	Typical Steppe	27	16.7	(10.6)	303.6	(360.8)
	Desert Steppe	29	11.0	(4.2)	90.7	(69.0)
2010	Meadow Steppe	92	46.0	(17.6)	398.8	(254.6)
	Typical Steppe	279	47.4	(16.9)	415.6	(207.4)
	Desert Steppe	117	27.0	(12.1)	132.5	(73.4)
2011	Meadow Steppe	44	52.7	(15.8)	176.1	(162.9)
	Typical Steppe	59	46.4	(17.9)	239.7	(186.2)
	Desert Steppe	32	28.1	(16.6)	95.0	(64.2)
	Desert	2	36.3	(23.8)	26.6	(6.6)
2012	Meadow Steppe	10	70.0	(12.2)	145.2	(48.3)
	Typical Steppe	53	65.5	(12.6)	206.1	(102.8)
2013	Meadow Steppe	5	3.3	(1.7)	137.6	(52.1)
	Typical Steppe	172	24.5	(24.8)	209.6	(143.0)
	Desert Steppe	55	7.0	(18.4)	89.7	(157.8)
	Desert	5	0.2	(0.1)	59.6	(16.1)
2014	Meadow Steppe	21	78.0	(9.8)	139.5	(51.6)
	Typical Steppe	20	65.8	(15.7)	141.1	(63.1)
2015	Meadow Steppe	7	55.7	(7.3)	120.2	(75.9)
	Typical Steppe	28	50.2	(17.3)	126.2	(99.8)
	Desert Steppe	2	25.0	(14.2)	43.6	(62.7)
2016	Meadow Steppe	29	70.0	(18.8)	213.2	(106.0)
	Typical Steppe	22	34.3	(23.2)	126.3	(68.8)
	Desert Steppe	18	9.2	(9.5)	90.0	(64.4)
	Desert	11	6.5	(5.4)	109.1	(100.3)

with transects moving away from the population centers to represent diverse vegetation structure. This is based on past research which suggests that degradation owing to grazing pressure would be greater in the mountain-meadow steppe complex, as compared to the desert steppe, and at intermediate levels in the typical steppe (Angerer et al., 2008). Transect samples were stratified by the dominant meadow-mountain, typical and desert steppe vegetation types to obtain representative ecological structure as well as the adjacent ecotones that border the steppe (e.g., understory communities in the forest steppe and desert vegetation types). Delineation of forest, meadow steppe, typical steppe, desert steppe types was based on a vegetation map jointly developed by the Institute of Botany, Chinese Academy of Sciences and the Institute of Botany, Mongolia (Wang et al., 2013; John et al., 2016).

Observed CC generally declined across the precipitation gradient with high values in the meadow steppe (45–78%), intermediate values in the typical steppe (34–50%) and low values in the desert steppe (10–26%) across the years (Table 1). Similarly, observed AGB across the growing season was the highest in the meadow steppe, with values ranging from 213.2 g m^{-2} in MG (2016) to 428.9 g m^{-2} in IM (2007). Typical steppe AGB measured across the growing season was highly variable, ranging from 126.3 ± 68.8 g m^{-2} in MG (2016) to 303.6 ± 68.84 g m^{-2} (2007) in IM (Table 1). Desert steppe AGB estimates varied from 89.96 to 94 g m^{-2} while desert AGB values were the lowest, ranging from 26.6 to 59.6 g m^{-2} (Fig. 1, Table 1).

2.3. Spatial data

Several remote sensing products were used to estimate the measures of land surface properties and scale-up in situ measurements to the region. MODIS data are especially suited for scaling up CC and AGB owing to it high revisit frequency, and ability to measure large areal extents. We used the *MODIS Nadir BRDF Adjusted Reflectance* (*NBAR*) (MCD43A4 V006) combined Terra and Aqua product to obtain surface reflectance (Schaaf, 2015) from NASA EOSDIS's data portal (https://earthdata.nasa.gov/). The 500 m resolution MODIS NBAR product provides 8-day composites of normalized reflectance that are corrected for bidirectional and atmospheric effects (Schaaf et al., 2002; Schaaf, 2015). The MODIS reprojection tool (MRT) was employed to mosaic nine MODIS tiles per 8-day period and project the surface reflectance data for July and August of 2000 through 2016 to the Albers Equal Area projection and WGS 84 datum. The surface reflectance data were cleaned of cloud and data artefacts using the MCD43A2 V006 quality assurance product. The derived MODIS VIs include proxies of vegetation cover, greenness and vigor such as NDVI, EVI (Huete et al., 2002) and enhanced vegetation index-2 (EVI-2) (Jiang et al., 2008). We also included water content indices such as the normalized difference water index (NDWI) (Gao, 1996), land surface water index (LSWI) (Xiao et al., 2002) and the normalized difference senescence vegetation index (NDSVI). The use of the visible and NIR domain is limited in water-limited ecosystems owing to the difficulty in distinguishing dry vegetation from background soil signature (Jacques et al., 2014). LSWI and NDSVI both use the SWIR band which is sensitive to changes in vegetation water content. We also used the inverse of MODIS NIR bands, after scaling MODIS NBAR Band 2 reflectance to 8-bit in order to obtain a reversed image (i.e., 255-NIR), as canopy height was found to be inversely related to NIR reflectance magnitudes (Table S1) (Qi et al., 2002; Marsett et al., 2006; Jacques et al., 2014). In order to reduce the dimensionality and to decrease the number of variables in rule-based modeling, we derived tasseled cap brightness, greenness and wetness components (TC_{bright}, TC_{green}, TC_{wet}) which serve as proxies of albedo, vegetation, and moisture, from the 500 m MODIS NBAR bands instead of using the NBAR reflectance directly in modeling (Lobser and Cohen, 2007).

We used the SRTMGL1 Global 1 arc *sec* (30 m resolution) V003 DEM (NASA-JPL, 2013) product to characterize elevation over the MP. We also obtained first order derivatives such as slope and aspect to aid in stratification. Categorical variables such as vegetation types were used to delineate forest, meadow steppe, typical steppe, and desert steppe types (Wang et al., 2013). The datasets listed above served as predictor variables to obtain wall-to-wall coverage of scaled up CC and AGB. We used the MODIS Land Cover Type 500 m product (MCD12Q1) to mask out forest and cropland cover classes using the University of Maryland classification scheme in order to confine the study to the grassland cover type.

We acquired total surface precipitation (PRECTOTCORR) and 2 m air temperature (T2M) from NASA's Modern-Era Retrospective Analysis for Research and Applications (MERRA) meteorological reanalysis dataset. The MERRA-2 reanalysis data with 0.5° × 0.67° resolution were acquired via the Goddard Space Flight Center simple subset portal (http://disc.sci.gsfc.nasa.gov/SSW/) (Rienecker et al., 2011; Bosilovich and Lucchesi, 2016) to obtain high quality, long-term precipitation data for 1981–2016. The monthly data were averaged to calculate MAP, the mean annual temperature (MAT), mean growing season precipitation (MGP), mean growing season temperature (MGT) and seasonal composites of spring (MAM) and summer (JJA) in order to explain the variability in CC and AGB variability.

2.4. Regression tree analysis and validation

We used an open source version of the Cubist (Quinlan, 1993) rule-based package in R (vers. 0.0.20) (Kuhn et al., 2017) to scale-up CC and AGB in situ measurements to the plateau scale using the MODIS and SRTM DEM derived data listed above. Cubist rule-based algorithms typically assign class membership through recursive partitioning of input datasets into homogeneous subclasses (Xiao et al., 2010). Previous studies suggest that: rule-based methods can account for non-linear relationships between observed and predicted variables, are more effective than multivariate linear regression, and are easier to interpret than neural networks (Huang and Townshend, 2003; Wylie et al., 2016). The Cubist method creates a RT where the terminal nodes are linear regression models.

Regression tree methods such as RF (Breiman, 2001) use recursive partitioning and each final node is associated with a single value. By contrast, Cubist develops a number of multiple linear regression sub-models, and each sub-model is associated with a set of rules (Xiao et al., 2008). A Cubist model is similar to a piecewise linear model with the exception that rules overlap each other. Cubist also differs from RF in that its predictive accuracy can be improved by combining with instance-based (similar training cases) or nearest neighbor's model to predict the target value of a new case using the average predicted values of the *n* most similar cases. Such composite models have been shown to be more accurate than rule-based models alone. Cubist can also generate committee models. Each committee model consists of a set of sub-models, each of which is associated with a set of rules. For each case, each member of the committee generates a prediction, and all the members' predictions are averaged to provide the final prediction.

Cubist has been used in the past to scale-up net ecosystem exchange (NEE) and gross primary production (GPP) to the conterminous United States using MODIS 500 m and 1 km resolution products (Xiao et al., 2008; Xiao et al., 2010). The MODIS derived datasets listed in section 2.3 were used as predictor variables to estimate and map 8-day composites of CC and AGB throughout the peak growing season (i.e., July, August). We also used elevation, slope and aspect as well as categorical variables (e.g., steppe type) as predictors to improve model prediction through stratification.

We validated the Cubist committee models by randomly dividing the data into training (80%) and testing (20%) samples for model calibration and model validation, respectively. In order to determine the model performance, we used the root mean square error (RMSE), the mean absolute error (MAE), mean absolute percentage error (MAPE), and coefficient of determination (R^2) to quantify goodness of fit and

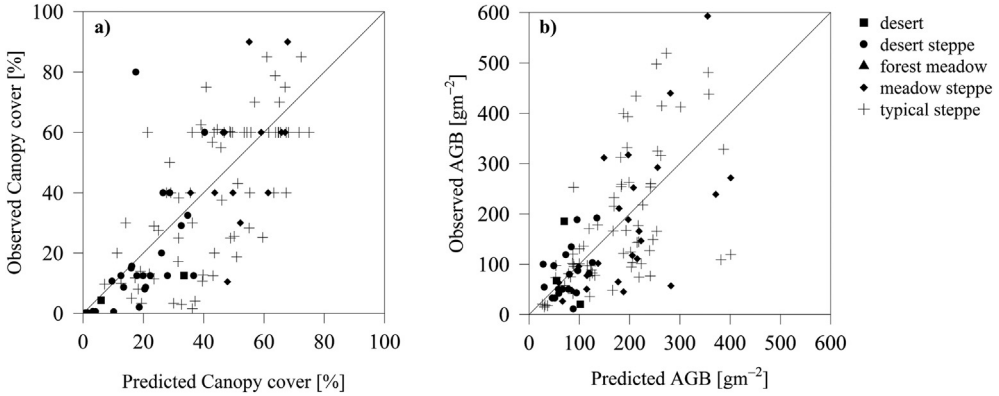

Fig. 2. Scatterplot of observed and predicted: a) canopy cover and b) aboveground biomass. The solid line depicts the 1:1 line between observed and predicted values.

model accuracy. We also calculated the root mean square error of validation (RMSEv) in order to compare with the standard error of regression (i.e., RMSE). A small difference between the two values indicates that the model is not overfitting (Andersen et al., 2005; Giannico et al., 2016). In addition, we calculated the relative RMSE, RMSEv and MAE expressed as percentage (MAPE), with lower values indicating lesser residual variance and higher model precision and accuracy. We evaluated the model performance using scatterplots of predicted vs observed CC and AGB. Variable importance (VarImp) analyses were conducted using the R package Caret (vers. 6.0–78) in order to assess the relative contributions of the predictor variables to the modeling process (Kuhn, 2017). Variables of importance are linear combinations of the predictor variables usage in the Cubist RT rule conditions and the linear models. We also constructed a Multiple Linear Regression (MLR) model through a step-wise regression using the predictive geospatial variables and the CC and AGB variables for comparison with the rule-based regression tree analysis.

2.5. Socioeconomic data and disturbance predictor variables

We obtained census data that includes total population at Level-2, county-level administrative divisions (*Soum* in MG, $N = 337$ and *Xiàn* in IM, $N = 90$). In addition, official estimates of total livestock population and livestock types (i.e., sheep, goat, cattle, and horses) were obtained from the National Statistical Office Yearbooks in MG. Similar data were obtained from statistical yearbooks and *Xiàn* level authorities in IM (Statistical Bureau of Inner Mongolia, 1989–2014). The annual livestock census in MG is only taken at the end of the year, whereas the livestock census in IM is collected twice a year (mid-year and year-end). Therefore, we ensured that only data from the end of the year were used for comparative purposes. Livestock and human population were normalized by area to obtain livestock and human population densities (LIV_D & POP_D). We calculated Euclidean distance (m) to larger towns that are provincial capitals of level-1 administrative units (*Aimags* or prefectures in MG and IM, respectively) as well as distance to level-2 administrative units, i.e., smaller towns or villages that serve as county (*Soum* or *Xiàn* in MG and IM, respectively) headquarters. We used the Mann-Kendall non-parametric trend tests to analyze the time-series of total livestock and population densities and the Theil-Sen method (Sen, 1968) for slope estimation for the study period. The distribution of slope trends at the *Soum*/county level was mapped to examine the variability of the predicted CC and AGB trends. The *ppcor* package in R was used to compute partial correlations between the scaled up CC/AGB estimates averaged at the county level, and climate and anthropogenic drivers after eliminating the effect of all other driver variables (Kim, 2015).

A time-series cross-sectional analysis accounted for the influence of livestock density, CC and AGB in both MG and IM. We employed a fixed effects model to account for time effects in the estimation. Both Lagrange multiplier and Hausman tests statistically support the suitability of the fixed effects model. The estimation model takes the following form:

$$Y_{it} = \alpha_i + \beta_1 X_{it} + e_{it} \quad i = 1, \ldots\ldots, N \qquad t = 1, \ldots\ldots, T \tag{1}$$

$$Y_{it} = \alpha_i + \beta_1 X_{it} + \beta_2 C_{it} * D_i + e_{it} \quad i = 1, \ldots\ldots, N \qquad t = 1, \ldots\ldots, T \tag{2}$$

where Y is a predicted AGB/CC, i is the *Soum*/county, t is a year from 2006 through 2016, α_i is an intercept, β is a scalar, e_{it} is a non-observable random term, and X is a set of independent variables. The independent variables consist of LIV_D, MAP, MAT, and D_i, regional dummy variables, (i.e., desert, typical, and meadow steppe). To control regional differences on the livestock density, we introduced $\beta_2 C_{it} * D_i$ as an interaction term between independent variable, LIV_D, and regional dummy in formula (2). By applying LIV_D on C_{it}—the interaction term can be regarded as an adjustment to the slope coefficient on LIV_D for different steppe types. We used the estimates of CC and AGB in the desert vegetation category as a reference baseline for the regional dummy.

3. Results

3.1. Model development and evaluation

Our predictive rule-based models for CC had NDSVI, NDWI, and TC_{bright} as variables of importance with a MAE of 10.26% (11%; MAPE) (Table S4) and consisted of five Cubist committee models made of 22 rule-based sub models (Appendix). The best predictive rule-based models for AGB had LSWI, NDVI, and NDWI as variables of importance, with a MAE of 59.83 g m^{-2} (9%) (Table S4) and consisted of five Cubist committee models made of 14 rule-based sub-models (Appendix).

Significant correlations were found in randomly selected CC and AGB predicted-observed pairs, which captured most of inter-annual and intra-season (JJA) variability and were statistically significant ($p < 0.05$) (Fig. 2). The models estimated CC and AGB reasonably well, considering the fact that the observations were from numerous sites, across diverse ranges of vegetation types, crossed climate and disturbance gradients and collected over multiple years. The model performance varied by site and vegetation type. The predicted-observed plots depicted a xeric-to-mesic gradient when stratified by desert, typical and meadow steppe. However, our CC model underestimated relatively high (observed) canopy cover in the desert steppe which is typical of shrub patches in a matrix of sparsely vegetated landscape dominated by xeric grass species (Fig. 2a, Fig. S3). The committee models also underestimated CC in some typical and meadow steppe sites with model performance tapering off at the 60% observed cover threshold. With a few exceptions, AGB was slightly underestimated by

Table 2
Prediction accuracy of canopy cover (CC) (%) and aboveground biomass (AGB) ($g\,m^{-2}$) by the models and validation using Cubist regression trees for the Mongolian Plateau.

Response variable	R^2	RMSE	RMSEv	Variables of importance
Canopy cover	0.71	13.73	14.44	NDSVI (66.5%), NDWI (58%), Tasseled cap-bright (50.5%)
AGB	0.62	85.87	76.87	LSWI (31%), NDVI (46.5%), Tasseled cap-bright (21.5%), NDWI (13%)

committee models in most typical and meadow steppe sites for values over 300 $g\,m^{-2}$ (Fig. 2b).

The Cubist committee models performed well in the prediction of CC with the best model consisting of predictive variables: NDSVI, NDWI and TC_{bright} (Table 2). The CC Cubist committee model performed better than the stepwise regression (R^2 of 0.71 and 0.63, respectively) (Table 2, Table S2). The AGB committee model also performed better than the stepwise regression model (R^2 of 0.62 and 0.40, respectively) (Table 2, Table S2). The committee model for AGB consisted of the following variables of importance: NDVI, LSWI, TC_{wet} and NDWI.

Cubist committee models were also developed for CC and AGB for the two political entities, MG and IM (Table 3). The CC committee models performed better at the political unit scale (MG and IM) compared to the entire plateau (Table 3). The AGB committee model had a greater predictive power for IM but decreased when the study extent was limited to MG (Table 3). The variables of importance for CC in MG and IM were $TC_{green,}$ and $TC_{bright,}$ as well as water content indices such as (i.e., NDWI and NDSWI). VIs and water content indices (i.e., EVI, NDVI, NDWI, $TC_{green,}$ and $TC_{wet,}$) were the best predictors in AGB committee models at the MG and IM scale.

3.2. Model validation

The validation of the predictive model showed that CC was estimated fairly well with an RMSE and $RMSE_v$ of 13.73% (14% relative RMSE) and 14.44% (16% relative $RMSE_v$), respectively at the plateau level (Table 2, Table S5). The AGB predictive model also performed well with an RMSE and $RMSE_{v,}$ of 85.87 $g\,m^{-2}$ (13%) and 76.87 $g\,m^{-2}$ (16%), respectively (Table 2, Table S5). The predictive model for CC had a higher predictive ability (R^2 = 0.73 and 0.77) in IM and MG, respectively, than at the plateau level, with IM having a lower RMSEv than MG (Table 3, Table S5). The models of CC had lower predictive ability for steppe vegetation types with the exception of desert steppe types (R^2 = 0.82).

The AGB predictive model at the level of the political unit explained some of the variation in MG (R^2 = 0.55) with an $RMSE_v$ of 56 $g\,m^{-2}$ (16%) (Table 3, Table S5). In contrast, the validity of the IM AGB predictive model was low, with a higher $RMSE_v$ of 119.64 $g\,m^{-2}$ (21%) (Table 3, Table S5). The predictive models of AGB at the steppe level had superior predictive ability, especially for the typical steppe type (R^2 = 0.72), with an $RMSE_v$ of 73.06 $g\,m^{-2}$ (17%) (Table 3, Table S5). Similarly, the AGB predictive model for the meadow steppe performed reasonably well with a lower $RMSE_v$ of 99.87 $g\,m^{-2}$ (19%) (Table 3, Table S5). In contrast, the AGB predictive models in the desert steppe had the highest $RMSE_v$ of 84.4 $g\,m^{-2}$ (33%) (Table 3, Table S5).

3.3. Canopy cover and AGB on the Mongolian plateau and environs

The inter-annual variability of CC and AGB varied across steppe types but was more pronounced in MG than in IM (Fig. S1 and Fig. S2). The spatial distribution of predicted CC and AGB (Fig. 3, Fig. 4) had high heterogeneity and varied along precipitation, latitudinal/temperature and elevation gradients (Table 1). The Mann-Kendall trends analysis of the July–August average for 8-day CC and AGB during 2000–2016) showed significant changes in the eastern provinces of MG, namely Dornod, Sukhbaatar and, Khentii (Fig. 5). This increase in CC and AGB was also manifested in central and western provinces of MG, including northern *Soums* of Ovorkhangai, Bayankhongor and Khovd and Bayan-O'lgii (Fig. 5). There was also a significant increase in CC and AGB along the desert ecotone margins in Ordos, Bayannur and Tongliao prefectures (Fig. 5a, b).

There was a significant decrease of CC and AGB in Baotou, Hohhot, Ulanqab, Hulunbuir prefectures, and in some counties of Xilingol, Hulunbuir Shi and Chifeng prefectures (Fig. 5a, b). Similarly, there was a significant decrease of CC and AGB along the border of Bulgan/Arkhangai provinces, and some *Soums* of Khovsgol, Uvs, and Khentii (Fig. 5a, b). A comparison between the averages of JA composites from 2000 to 2004 and 2012–2016 of CC and AGB also showed similar changes when differencing was used (Fig. S4).

3.4. Climate forcing and anthropogenic drivers

At the MP scale, the partial correlation analysis showed that predicted CC had a moderate to high correlation with MAP and MGP (r_p = 0.57 and 0.56, *p-value* < 0.05), with a greater correlation to summer precipitation, PJJA than to spring precipitation, PMAM (r_p = 0.52, Table 4). When the effects of temperature and anthropogenic drivers (e.g., LIV_D, POP_D) were controlled for, the moderate correlation remained mostly the same. A higher correlation existed between CC and MAP, MGP in MG as compared to IM, but with a greater correlation to summer precipitation, PJJA than to spring precipitation, PMAM (Table 4). The partial regression of CC with MAT and MGT showed a greater negative correlation at the IM and MG scale compared to the plateau level. This negative correlation remained when partial regression was controlled for by precipitation and anthropogenic drivers. This negative correlation between CC and annual/seasonal indices of temperature was greater for MG than for IM (Table 4).

CC had a weak, positive correlation with LIV_D in IM and negatively correlated with distance to cities and towns in MG.

Table 3
Summary of prediction accuracy of canopy cover (CC) (%) and aboveground biomass (AGB) ($g\,m^{-2}$) from model development and validation using Cubist regression trees stratified by political unit and vegetation type.

Variable	Category	R^2	RMSE	$RMSE_v$	Variables of Importance
CC	MG	0.77	13.08	14.53	Tasseled cap-green (44.5%), inverse NIR1 (25.5%), Tasseled cap-bright (42.5%)
(%)	IM	0.73	11.44	13.58	Tasseled cap-green (45%), NDWI (48.5%), NDSVI (46%)
	Meadow Steppe	0.43	15.90	15.32	Elevation (30%), EVI (10%), NDVI (0%)
	Typical Steppe	0.46	17.32	17.49	NDSVI (51.5%), inverse NIR1 (38.5%), Tasseled cap-bright (38.5%)
	Desert Steppe	0.82	4.79	17.93	NDWI (34.5%), LSWI (32.5%), inverse NIR1 (20%)
AGB	MG	0.55	63.15	56.00	EVI (30%), NDVI (20%), NDWI (20%)
($g\,m^{-2}$)	IM	0.75	73.80	119.64	Tasseled cap-green (38%), Tasseled cap-wet (19.5%), NDVI (55%)
	Meadow Steppe	0.52	109.85	99.87	EVI (20%), Inverse NIR1 (20%), Elevation (20%)
	Typical Steppe	0.72	72.64	73.06	Tasseled cap-green (38%), LSWI (26%), NDWI (6%)
	Desert Steppe	0.66	45.49	84.44	NDVI (42%) NDWI (38%), inverse NIR1 (29%)

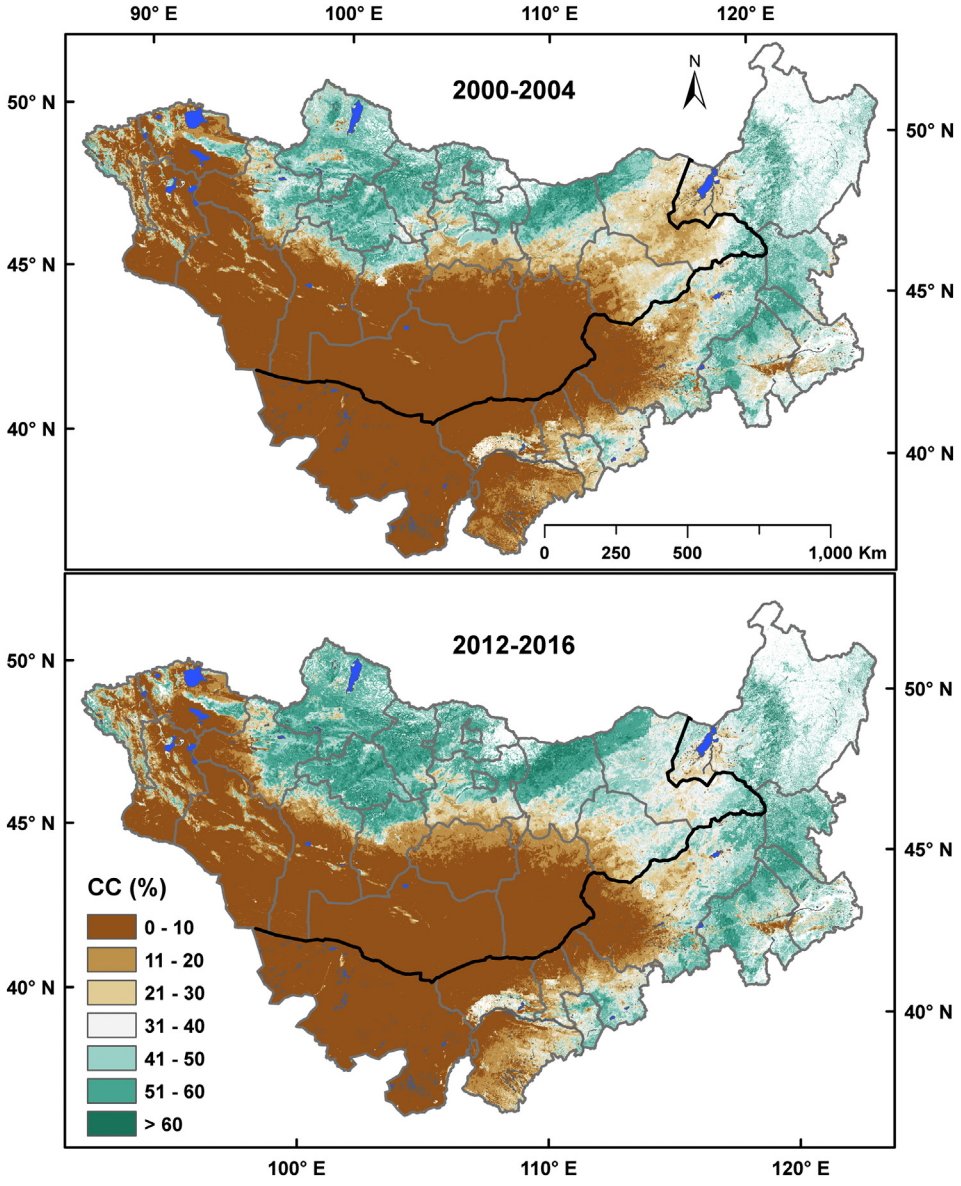

Fig. 3. MODIS-derived peak season canopy cover (CC, %) over the Mongolian Plateau and its environs. Maps describe July–August composites averaged over: a) 2000–2004; and b) 2012–2016. Areas under forest and cropland cover were masked out using MODIS-derived MCD12Q1 land cover product.

Predicted AGB at the plateau level showed a stronger correlation with MAP, MGP and summer precipitation compared to spring precipitation and this relationship held when the effects from other variables were controlled for (Table 4). The AGB also showed a stronger negative relationship with MAT and spring temperature as compared with MGT or summer temperature. The AGB was positively correlated with LIV_D both in IM and MG as well as the MP scale. At the MP scale, CC and AGB were negatively correlated with distance to cities and towns. This negative correlation was stronger in MG even when precipitation and temperature were controlled for. A weaker negative correlation was found between CC and AGB and distance to cities in IM (Table 4).

A cross-sectional analysis at the county level found that LIV_D exhibited a negative relationship with CC and AGB in both IM and MG (Model (1), (3), (5) and (7) (Table 5). This significant negative relationship was stronger for CC and AGB in MG than in IM. Furthermore, this relationship also held in models with the interaction term (Model (2), (4), (6), and (8) (Table 5).

4. Discussion

4.1. Gridded CC and AGB estimates of the Mongolian Plateau and environs

There exist very few gridded and scaled-up estimates of AGB and CC in the Mongolian Plateau and its adjacent regions. Some efforts were made at smaller extents and are limited to either Mongolia (Fernández-Giménez et al., 2017), Inner Mongolia (Zhang et al., 2014), a province within Inner Mongolia (e.g., Xilingol, (Xie et al., 2009) or to a single ecosystem type (e.g., temperate deserts, (Zhang et al., 2016). By contrast, we extensively measured both CC and AGB across the Mongolian Plateau, and generated gridded CC and AGB estimates for the entire region.

Our predictive models provide reasonable estimates of CC and AGB during the active growing season over a significant range of values 0–70% and 0–400 $g\,m^{-2}$, respectively (Table S6). These estimates are representative of the typical range of Mongolian grasslands in IM (i.e., 154.8 ± 17.1 $g\,m^{-2}$), the Eurasian steppe and semiarid regions worldwide (Kang et al., 2013; Zhang et al., 2014; Liang et al., 2016). Our predicted AGB estimates for the meadow steppe

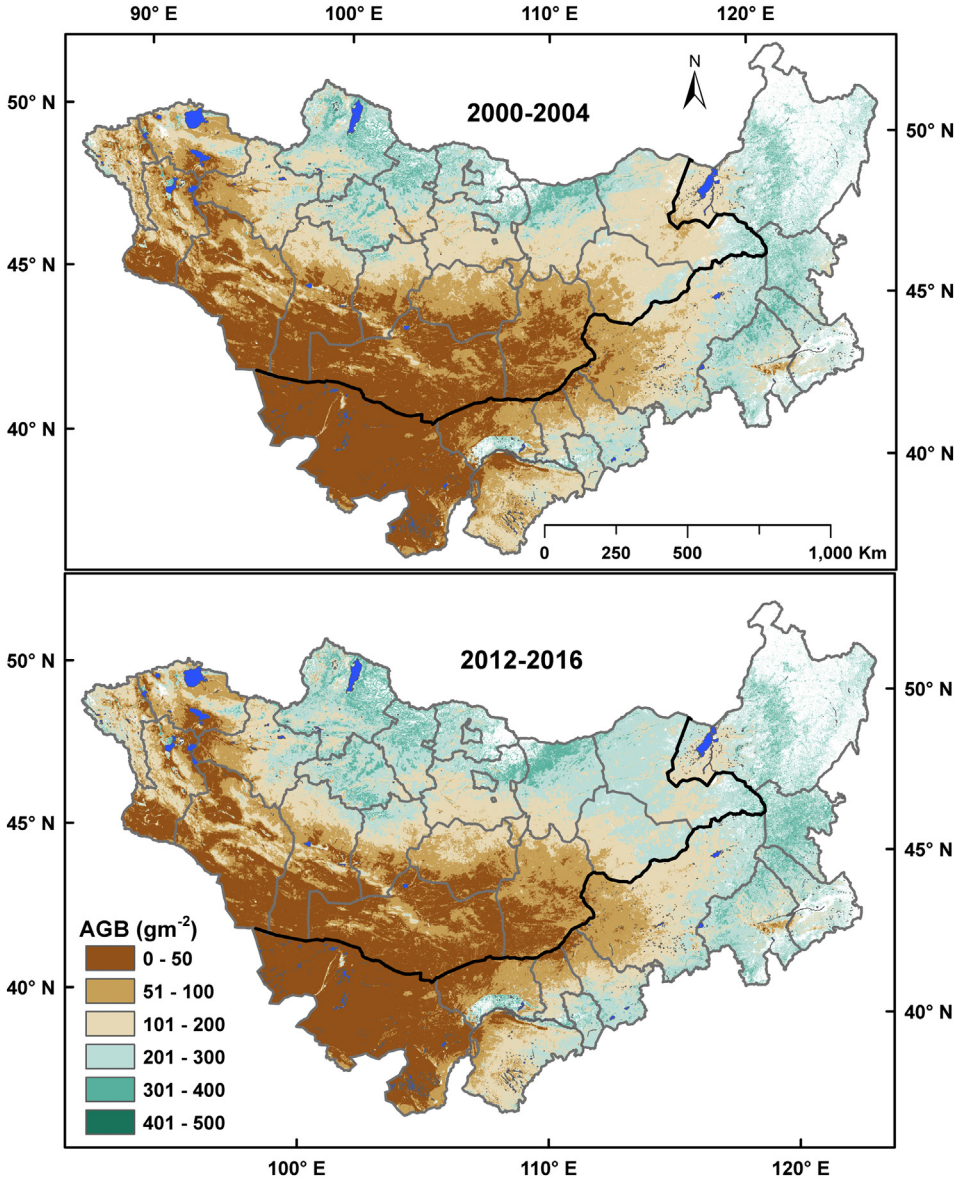

Fig. 4. MODIS-derived peak season aboveground biomass (AGB, g m^{-2}) over the Mongolian Plateau and its environs. Maps describe July–August composites averaged over: a) 2000–2004; and b) 2012–2016. Areas under forest and cropland cover were masked out using MODIS-derived MCD12Q1 land cover product.

(270.4 ± 79.7 g m^{-2}) were consistent with estimates of AGB from large area transects in IM, (228.7 ± 28.6 g m^{-2}) (Kang et al., 2013) and scaled up estimates in adjoining temperate grasslands in southern Qinghai (274.5 ± 53.4 g m^{-2}) (Liang et al., 2016). Similarly, our typical steppe estimates (173 ± 71.0 g m^{-2}), also agreed with estimates from large area transects in (162.8 ± 17.3 g m^{-2}) (Kang et al., 2013) and scale-up studies in (149.3 ± 90.4 g m^{-2}) (Xie et al., 2009) in IM. Our estimates for the desert steppe (64 ± 37.4 g m^{-2}) compared favorably with other assessments conducted in the region including measured estimates (42 ± 20 g m^{-2}) (Khishigbayar et al., 2015) in MG and scaled-up estimates (66 ± 72 g m^{-2}) (Zhang et al., 2016) in MG and IM. Although these previous studies were based on either field measurements, scaling-up efforts at the provincial scale or for a single biome (i.e., temperate desert), these comparisons demonstrate that our gridded CC and AGB estimates are reasonable in magnitude. Our data products allow us to examine the spatial patterns, seasonality, and interannual variability of CC and AGB for the entire Mongolian Plateau.

Our predicted estimates of CC for meadow, typical and desert steppe were 55.1 ± 11.5%, 26.8 ± 14.8%, and 4.06 ± 5.8%, respectively. One of the few, comparable MODIS-derived CC products was developed over Tibetan Plateau with CC estimates ranging from 40% in the montane steppes/alpine steppes of Gansu and Qinghai province, to 60% in the *Kobresia pygmaea* meadows in the Tibetan Autonomous Province (Lehnert et al., 2015). Another MODIS-derived CC dataset was developed for the temperate deserts of Central Asia and reports a higher CC range of 13 ± 16% as compared to our desert steppe CC estimates of 4 ± 5.8% (Zhang et al., 2016). They also reported a CC estimate of 21 ± 12% for their temperate semi-shrub and dwarf semi-shrub complex (including *Artemisia* spp), which is within the range of our typical steppe CC estimates of 26.8 ± 14.8%.

Our 500 m scaled up estimates from 2000 to 2016, compare favorably with coarse-scale (0.5 × 0.5°) gridded estimates of AGB, obtained from process-based models that covered the entire Mongolian Plateau. This study, based on the terrestrial ecosystem model, reported a mean net primary production (NPP) of 339 ± 72 g C m^{-2} yr^{-1} during the 1990s, which was higher than the *Carnegie-Ames*-Stanford Approach model estimates (290 g C m^{-2} yr^{-1}) for IM over a longer time period from 1982 to 2002 (Lu et al., 2009). A study used Cubist RT to upscale spatial and temporal estimates of net ecosystem production from a network of flux towers in temperate grasslands across IM and Gansu

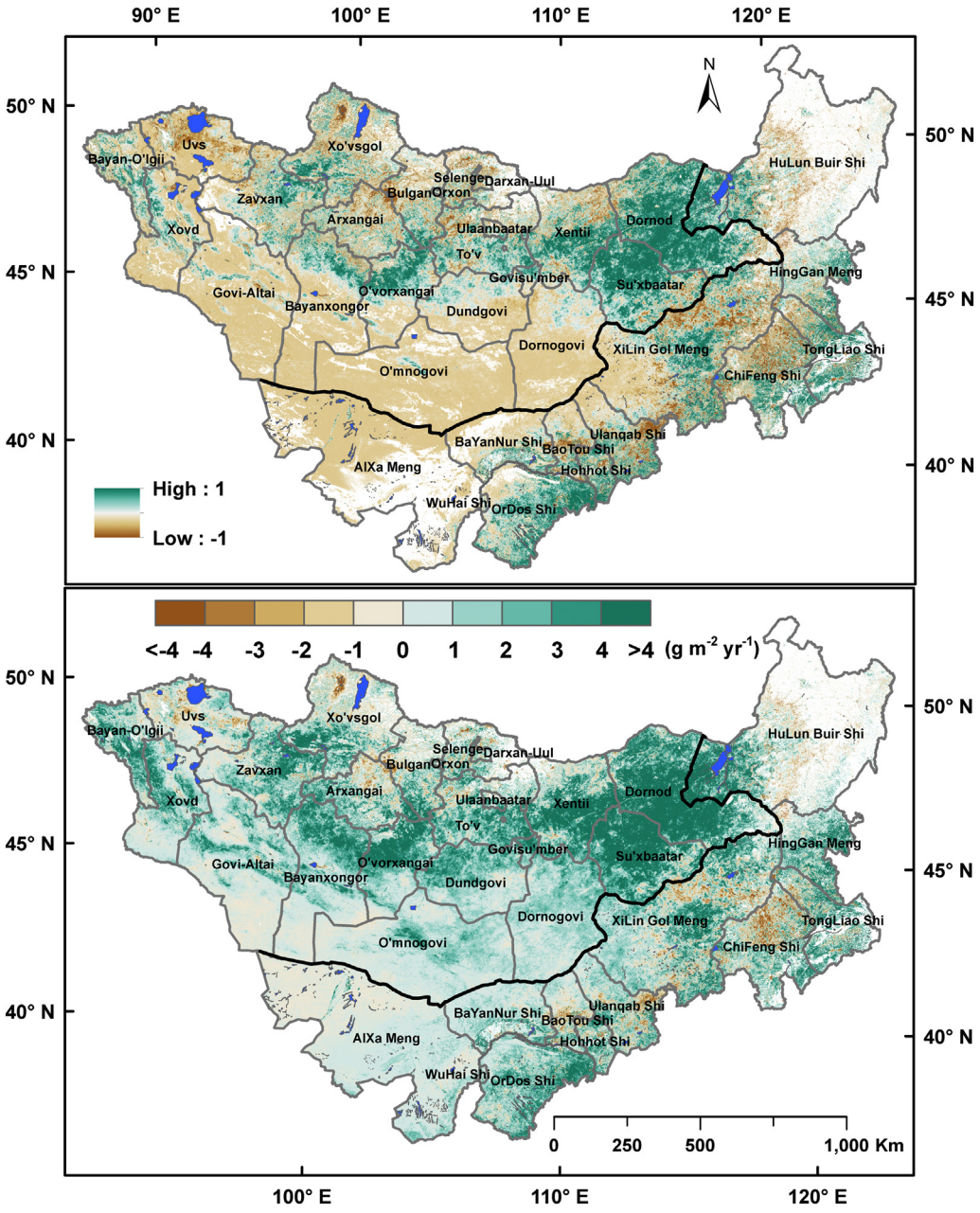

Fig. 5. Spatial changes in slope trends (2000–2016) of: a) canopy cover (CC, %); and b) aboveground biomass (AGB, g m^{-2}) derived from metrics based on MODIS MCD43A4 NBAR surface reflectance and ancillary variables on the Mongolian Plateau and its environs. Areas under forest and cropland cover were masked out using MODIS-derived MCD12Q1 land cover product.

province, China (2000 − 2010) and reported a growing season NEP range of 200–300 g C m^{-2} with RMSE of 0.31 g C m^{-2} d^{-1} (Zhang et al., 2014). Another study that focused on grasslands and croplands in the Great Plains Ecosystems of the United States also scaled up NEP from EC towers to MODIS NDVI using Cubist RT (Wylie et al., 2016). They reported an RMSE of 0.62 g C m^{-2} d^{-1} and 1.01 g C m^{-2} d^{-1} for grassland and croplands, with three and five committee models respectively.

It remains challenging to scale-up CC and AGB in water-limited ecosystems with large areal extent and high inter-annual variability, like the MP. Statistical models based on a suite of VIs derived from satellite sensors can have a high correlation with CC or AGB during a specific phenology period and location. However, model performance can drop significantly when site level estimates are scaled up to large areas, owing to high spatial heterogeneity of cover types, seasonal variability and species/community diversity within a cover type. We found a relatively high correlation in our predictive models against training data, but the model performance dropped on the test dataset when the validation was performed—with the exception of the AGB and CC predictive models across the plateau. Some sources of error include the spatial mismatch between the in situ sample plots and the 500 m MODIS pixels. Positional accuracy is less likely to be a major contributor to error, given the 500 m pixels.

Vegetation indices like NDVI and RVI have often been used to estimate AGB at regional scales on semiarid ecosystems such as the Mongolian Plateau and the Sahel. However, they have been criticized for saturating when vegetation cover is dense and are also sensitive to the soil background signature and shadows at < 50% cover (Huete et al., 2002). Stratified random sampling of different steppe types has the potential to improve CC and AGB estimates owing to high

Table 4
Partial regression coefficients between the predicted canopy cover (CC), above ground biomass (AGB) and climate factors of mean annual precipitation (MAP), mean annual temperature (MAT), mean growing season precipitation and temperature (MGP; MGT), seasonal precipitation and temperature for spring and summer (MAM; JJA), anthropogenic drivers represented by total livestock and population densities (LIV_D; POP_D) and distance to cities and towns in IM and MG (D_city; D_town).

ALL	% cover		MAP	MGP	PMAM	PJJA	MAT	MGT	TMAM	TJJA	LIV_D	POP_D	D_city	D_town
		default	0.57	0.56	0.46	0.52	−0.32	−0.28	−0.30	−0.26	0.16	0.23	−0.11	−0.17
		Prec.					−0.30	−0.26	−0.29	−0.24	0.12	0.19	−0.09	−0.16
		Temp.	0.57	0.55	0.45	0.52					0.16	0.23	−0.11	−0.16
		Anthro	0.57	0.56	0.46	0.52	−0.32	−0.28	−0.30	−0.26				
	AGB	default	0.62	0.61	0.46	0.57	−0.24	−0.20	−0.23	−0.20	0.16	0.26	−0.12	−0.12
		Prec.					−0.22	−0.18	−0.21	−0.17	0.13	0.22	−0.10	−0.10
		Temp.	0.62	0.60	0.46	0.57					0.16	0.26	−0.12	−0.11
		Anthro	0.62	0.61	0.46	0.57	−0.25	−0.20	−0.23	−0.20				
IM	% cover	default	0.58	0.56	0.46	0.53	−0.33	−0.28	−0.31	−0.27	0.17	0.25	−0.11	−0.18
		Prec.					−0.31	−0.27	−0.29	−0.25	0.13	0.20	−0.09	−0.17
		Temp.	0.57	0.56	0.45	0.52					0.17	0.25	−0.11	−0.18
		Anthro	0. 58	0.56	0. 46	0.53	−0.33	−0.28	−0.31	−0.27				
	AGB	default	0.62	0.61	0.46	0.57	−0.26	−0.21	−0.24	−0.20	0.18	0.28	−0.12	−0.12
		Prec.					−0.24	−0.19	−0.22	−0.18	0.14	0.24	−0.10	−0.11
		Temp.	0.62	0.60	0.46	0.57					0.18	0.29	−0.11	−0.12
		anthro	0.62	0.61	0.46	0.57	−0.26	−0.21	−0.25	−0.21				
MG	% cover	default	0.62	0.60	0.48	0.54	−0.38	−0.33	−0.36	−0.30	0.22	0.32	−0.15	−0.25
		Prec.					−0.39	−0.33	−0.31	−0.26	0.18	0.29	−0.13	−0.22
		Temp	0.61	0.59	0.48	0.54					0.21	0.31	−0.15	−0.25
		Anthro	0.62	0.60	0.48	0.54	−0.38	−0.33	−0.36	−0.30				
	AGB	default	0.64	0.63	0.48	0.57	−0.37	−0.32	−0.35	−0.30	0.19	0.28	−0.15	−0.21
		Prec.					−0.38	−0.32	−0.34	−0.31	0.29	0.28	−0.12	−0.19
		Temp.	0.63	0.62	0.47	0.56					0.15	0.25	−0.14	−0.21
		Anthro	0.64	0.63	0.48	0.57	−0.37	−0.32	−0.35	−0.30				

heterogeneity in plant community structure and environmental conditions. Our predictive model estimates of CC and AGB were constrained by low density and a relatively limited sampling of xeric vegetation types within the desert steppe and desert biome. We also limited our sampling to herbaceous vegetation and did not sample forests. We attempted to account for intra-seasonal vegetation dynamics and inter-annual variability by synthesizing data from several annual field campaigns sampled across the peak growing season. This multi-year synthesis of in situ samples not only enabled wall-to-wall modeling of spatially-explicit herbaceous CC and AGB and provided a record of vegetation dynamics across the plateau, but also helped to offset the limited number of sites sampled per year and the small plot size. Most scale-up studies in the region are limited in scale and extent and were conducted over a single field season or limited to a few sites. Hence, our work is unique in its contribution to our understanding the state and trends in spatial heterogeneity of CC and AGB on the plateau.

Table 5
Cross-sectional analysis of the time-series on the impact of livestock density to AGB and CC while considering regional effects, interaction term between livestock density and steppe types, temperature and precipitation fixed effect, and annual fixed effects.

		AGB ($g\,m^{-2}$)				CC (%)			
		(1) IM	(2) IM	(3) MG	(4) MG	(5) IM	(6) IM	(7) MG	(8) MG
Livestock density		−0.65***	−0.62	−1.09***	206.65***	−0.16***	−0.18**	−0.27***	44.99***
		(0.19)	(0.38)	(0.19)	(19.24)	(0.03)	(0.06)	(0.04)	(3.73)
Regional effects (dummy)	Desert steppe	−8.39	−8.66	−6.72***	18.81***	−8.08***	−9.79***	−4.49***	1.08*
		(8.17)	(11.17)	(2.22)	(3.32)	(1.34)	(1.83)	(0.43)	(0.64)
	Typical steppe	168.73***	94.66***	26.13***	54.56***	10.29***	10.08***	5.27***	11.78***
		(11.22)	(7.59)	(2.31)	(3.51)	(1.15)	(1.24)	(0.45)	(0.68)
	Meadow steppe	109.56***	148.11***	68.80***	98.81***	20.80***	19.91***	22.07***	28.19***
		(8.08)	(10.81)	(2.66)	(3.78)	(1.57)	(1.77)	(0.52)	(0.73)
Interaction terms (Regional effects * Livestock density)	Desert steppe	–	0.56	–	−204.76***	–	1.09	–	−44.83
			(5.16)		(19.25)		(0.85)		(3.73)
	Typical steppe	–	−0.02	–	−206.67***	–	0.02	–	−45.63**
			(0.44)		(19.23)		(0.07)		(3.73)
	Meadow steppe	–	−1.99	–	−207.68***	–	0.43	–	−45.19***
			(2.33)		(19.23)		(0.38)		(3.73)
Observations		1200	1200	5379	5379	1200	1200	5379	5379
R-squared		0.64	0.64	0.78	0.78	0.72	0.72	0.85	0.85
Degree of freedom		1079	1076	5358	5355	1079	1076	5358	5355
Temperature - Precipitation Fixed-effects		YES	YES	YES	YES	YES	YES	YES	YES
Time fixed-effects		YES	YES	YES	YES	YES	YES	YES	YES

Notes: Standard errors in parentheses. *** $p < 0.01$, ** $p < 0.05$, * $p < 0.1$. As an unbalanced panel data, the (1), (2), (3), and (4) AGB panel models are composed of (n = 80, T = 15, N = 1200), (n = 80, T = 15, N = 1200), (n = 317, T = 14–17, N = 5379), and (n = 317, T = 14–17, N = 5379), respectively. The (5), (6), (7), and (8) CC panel models are composed of (n = 80, T = 15, N = 1200), (n = 80, T = 15, N = 1200), (n = 317, T = 14–17, N = 5379), and (n = 317, T = 14–17, N = 5379), respectively.The reference of regional effect dummy is Desert. Temperature - Precipitation fixed-effect include Mean Annual Precipitation (MAP) and Mean Annual Temperature (MAT). The models include time fixed-effects to control annual variability. The models (1), (3), (5), and (7) are models based on the formula (1). The models (2), (4), (6), and (8) have an interaction term controlling the regional impacts on the livestock density.

Water content indices like NDWI, NDSVI, and LSWI and proxies of productivity like EVI, optimized for low cover conditions, were consistently chosen as variables of importance for CC and AGB at different extents (Huete et al., 2002; Jiang et al., 2008). We leveraged the utility of water content indices such as NDWI, LSWI and NDSVI, all of which use the MODIS SWIR bands to discern the difference between green vegetation and bare soil/litter signatures, thus enabling us to successfully explain most of the variance in CC and AGB (Table S1) (Marsett et al., 2006; Zhang et al., 2016). In order to reduce dimensionality and computational complexity, we used TC_{green}, TC_{bright}, and TC_{wet}, components instead of using all seven MODIS NBAR reflectance bands. The TC components enhanced the predictive ability of our rule-based models at both the plateau and steppe-type extents.

Most scale-up studies in the region primarily used NDVI-based predictive models (Xie et al., 2009; Zhang et al., 2016). Our CC and AGB RT-based predictive models (Table 2, Table 3) differed in accuracy from previous scaled up estimates in the region which differed greatly in methods and extent of study. A study in the Xilingol prefecture compared the use of artificial neural network (ANN, $R^2 = 0.81$, RMSE = 60) and multiple linear regressions ($R^2 = 0.59$, RMSE =74) in modeling biomass from Landsat TM scenes and produced a higher predictive accuracy than our analysis. However, the only vegetation index used was NDVI which can be a limitation in water limited ecosystems with sparse cover. In another study, AVHRR NDVI3g and MODIS NDVI were evaluated in their ability to obtain forage estimates across MG (Fernández-Giménez et al., 2017). Observed AGB collected at 300 sites in MG were regressed with AVHRR NDVI3g ($R^2 = 0.79$, RMSE = 22.5) and MODIS NDVI ($R^2 = 0.70$, RMSE = 16.4). However, the validation R^2 for GIMMS3g was 0.52, with an RMSE of 19.6.

A study on the CC and AGB in temperate deserts across Central Asia evaluated CC models based on NDVI ($R^2 = 0.56$, RMSE = 6.67), EVI ($R^2 = 0.61$, RMSE = 7.46) and three-band maximal gradient difference (TGDVI) ($R^2 = 0.73$, RMSE = 7.77) (Zhang et al., 2016). The authors found a wide range of predictive accuracy that overlapped with our study, but the methods were based on OLS linear regression that is sensitive to outliers. Our study compared favorably with a CC scale-up study in IM grasslands, based on linear un-mixing of VIs which reported model accuracy for NDVI ($R^2 = 0.66$, RMSE = 19.8), and ratio vegetation index (RVI) ($R^2 = 0.58$, RMSE = 24.8), respectively (Li et al., 2014). Another CC scale-up study over the Tibetan Plateau evaluated the use of several modeling methods on MODIS NBAR reflectance, which included support vector machine (SVR) ($R^2 = 0.91$, RMSE = 5.59), Partial Least Squares ($R^2 = 0.86$, RMSE = 8.20), linear un-mixing ($R^2 = 0.88$, RMSE = 12.65), and spectral angle mapper ($R^2 = 0.59$, RMSE = 8.00) (Lehnert et al., 2015). The authors suggested that methods such as SAM and linear un-mixing, which depend on in situ spectral end members, were inferior to advanced multivariate methods such as PLSR or machine learning methods. A study based in the United States which predictive models of urban forest cover and impervious surface area derived from Landsat reflectance and tasseled cap data found that SVR and Cubist consistently outperformed Random Forest (Walton, 2008).

4.2. Climatic, topographic and anthropogenic controls on CC and AGB

The response of vegetation to climate drivers on the MP is highly variable owing to the differential response of steppe types (John et al., 2016). Our results indicate that precipitation explained most of the variability of CC and AGB on the MP (Table 4). Mountain ranges surround the MP and play a major role in limiting moisture (Hilker et al., 2014). For example, the Northeast monsoon is limited by the Greater Hinggan Mountains in the East. The Mongol Altai and Gobi Altai to the south, the Khangai Mountains of Central Mongolia and the Sayan Mountains to the north further modify the regional climate system. The Siberian anticyclone determines the severity of winter and precipitation rates and also plays an important role in influencing the spatial distribution of CC and AGB (Hilker et al., 2014). Our CC and AGB maps depict the environmental gradient across the MP and reflects the northeast-southwest precipitation gradient in Inner Mongolia (Fig. 3, Fig.4). The maps also depict a latitudinal gradient that extends northward and includes steppe type transitions (i.e., desert-typical-meadow-forest steppe), which agrees with other regional studies (John et al., 2016; Zhang et al., 2016). Ongoing climate change might stimulate and facilitate future vegetation succession, leading to uncertainty in net carbon sequestration in semiarid ecosystems of the MP and Asian drylands (Shao et al., 2013). The strong influence of summer precipitation and temperature along with elevated CO_2 on AGB over the MP may benefit herbaceous, C3 plants which are the dominant communities in the meadow steppe. The desert steppe conforms to the non-equilibrium model of rangeland dynamics, where ecosystem function depends on both the amount and timing of rainfall and is thus vulnerable to increased inter-annual variability in precipitation trends. The meadow steppe, on the other hand, is governed by the equilibrium model where rangeland degradation can be explained by herbivory; and is thus sensitive to livestock density (Fernández-Giménez and Allen-Diaz, 1999; Wesche et al., 2010).

A combination of the large, spatial extent, the inter-annual variability of precipitation and temperature over a 15-year period and the rapid changes from human-induced land cover/use make the validation of CC and AGB a daunting task (Fig. 5, Fig. S1, Fig. S2, Fig. S4). Our non-parametric trend analysis of CC and AGB found significant, positive trends that are consistent with the findings of other independent studies in the region which also used MODIS data over a decade and 30-year AVHRR records (Eckert et al., 2015; John et al., 2016). These increasing or stable CC or AGB trends could be attributed to a decrease in grazing pressure in provinces on the periphery such as Dornod, Sukhbaatar and Bayan-Olgii as well as remote *Soums* in the Khangaai provinces of Ovorkhangai and Bayankhongor (Fig. 5). This decrease in grazing pressure could result from decreased population density, which in turn can be explained by migration to provincial centers and towns from outlying villages (Fig. 6) (John et al., 2016). On the other hand, the provinces of the North Central region and portions of the Khangai Mountains have the highest livestock densities in MG, but have stable or decreasing trends in CC and AGB (Fig.5, Fig. 6). There has been a decline in the number of herders, herding households and livestock-owning households in MG and IM, with a concomitant increase in service industries near cities and towns (Fernández-Giménez et al., 2017), though the overall livestock density has increased (Chen et al., 2015b). Negative trends in CC and AGB in MG could be explained by the accelerated growth of Ulaanbaatar (Fig. 6b), and anthropogenic modification, including increased grazing pressure in North Central Mongolia and increased sedenterization by herders (Eckert et al., 2015; Fan et al., 2016; John et al., 2016; Fernández-Giménez et al., 2017). Negative trends in IM and MG could also be explained by the growth of provincial cities (prefecture and *Aimag* centers) and the disturbance exerted on the surrounding landscape by their urban footprint. These cities have improved infrastructure and provide access to a range of services, including education, health and economic opportunities (Chen et al., 2015b; Park et al., 2017). The transition of MG into a market economy from 2000 to the present has led to an rise in mining in some provinces (Fernández-Giménez et al., 2017). The decrease in biomass trends in the western province of Uvs province can be explained by coal mines near the city of Ulangom, Coal mines in Nalaikh east of Ulanbaatar, gold mines in the northern province of Selenge (McIntyre et al., 2016), copper and coal mines in the southern Mongolian province of Omnogovi (Jackson, 2015).

The effects of extreme climate events on coupled human-natural systems are more pronounced in MG than in IM (Chen et al., 2015a; John et al., 2016; Park et al., 2017). Vegetation cover and AGB in the MP has been strongly influenced by the combined effects of prolonged drought and *dzuds* in the last decade (Fig. S1, Fig. S2) (John et al., 2013b). Droughts have amplified the effects of *dzud* through reduced

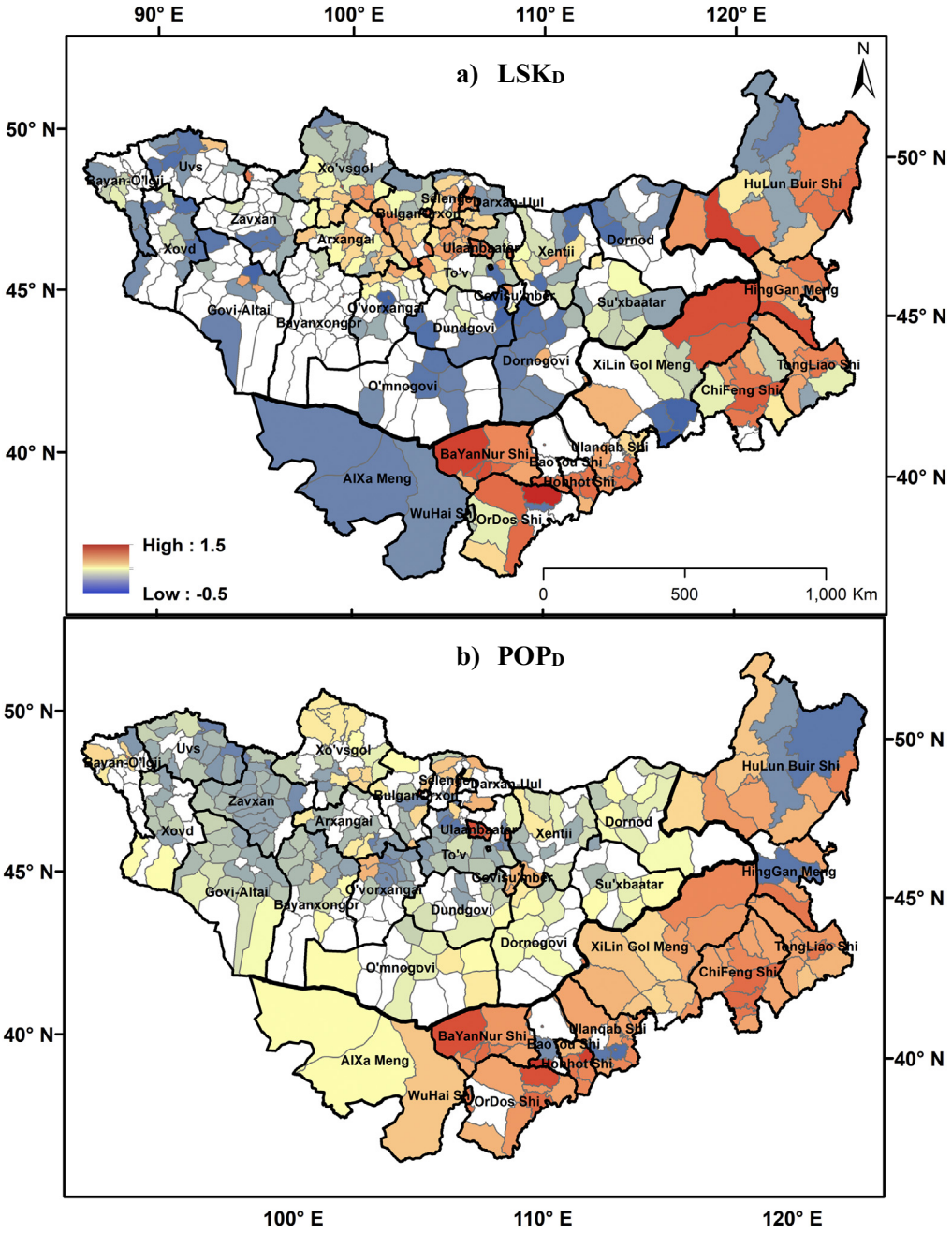

Fig. 6. Spatial changes in the Theil-Sen slope trends of: a) LSK_D – total livestock density, and b) POP_D – total population density. The legend shows positive slope trends in red and negative slope trends in blue. Blank *Soums or Xiàn* (counties) have slope trends that are not significant. (For interpretation of the references to color in this figure legend, the reader is referred to the web version of this article.)

forage availability and have led to record livestock mortality in 2003 and 2010 (Rao et al., 2015; Fernández-Giménez et al., 2017). The drought-*dzud*s also drove rural-urban migration in MG between 2000 and 2014, with a 9.2% increase in the urban population. This was followed by the 2011–2014 wet period, which fueled a further increase in livestock stocking rates and led to a cyclical trend that was closely coupled with extended wet and dry periods. This trend was a continuation of the rapid increase in stocking rates following the collapse of the former Soviet Union in 1991 (Chen et al., 2015b; John et al., 2016). Livestock herds in the Collective era had relatively constant populations with herd mobility facilitated by state supported infrastructure that included watering points and shelters in remote areas. However, studies suggest that, there had been substantial changes in the spatiotemporal patterns of grazing, post 1991, due to the increase in stocking rates, which resulted from the increased demand of the new market economy. The lack of state support led to the deterioration of herding infrastructure owned by collectives with no state regulation of stocking rates or herd mobility. Post 2000, organized groups of herders have begun to regulate herding movements, especially long distance migrations, in response to drought-*dzuds*, further adding to complexity in spatial heterogeneity of grazing patterns (Fernández-Giménez et al., 2017). Easier access to social goods and services has led to the sedenterization of herders near towns and villages, leading to degraded pastures in close proximity to population centers (Fernández-Giménez et al., 2017). Our results offer further proof of the ecological footprint of sedenterization, especially around towns that are provincial (*Aimag*) centers and villages (*Soum* headquarters) (Table 4) (Fig. 6). Our cross-sectional analysis confirms previous findings regarding the negative

impact of LIV_D on AGB and CC, and also confirms that the steppes in MG are more sensitive to LIV_D than those in IM (Table 5) (Chen et al., 2015b; John et al., 2016). The impact of livestock density on CC and AGB was lesser in IM than in MG and could be attributed to greater herding infrastructure and pastoral management in IM (Chen et al., 2015a; Chen et al., 2015b). We also found that the LIV_D had a greater impact on the meadow steppe as compared to other steppe types (Table 5). Our findings validate past research which suggests that degradation owing to grazing pressure was greater in the mountain-meadow steppe complex as compared to the desert steppe, and at intermediate levels in the typical steppe (Angerer et al., 2008; Karnieli et al., 2013). This implies that the sustainable rangeland management in MG and IM is an urgent issue and needs to be location specific. AGB and CC trends were not explained solely by LIV_D but by a combination of factors, including precipitation trends and distance to urban/built up areas. This also confirms the findings of recent studies that some of the recent land cover change on the plateau was attributed to the increased urban footprint of cities and major towns in IM and MG (Fan et al., 2016; John et al., 2016; Park et al., 2017).

Positive trends in CC and AGB in Xilingol, Ulanqab and Baotou prefectures in IM could also be explained by the implementation of the Returning Farmlands to Forest and Grassland Project (also known as Grain to Green program) where marginal agricultural land was converted to grasslands (Uchida et al., 2005). Similarly, the Beijing and Tianjin Sandstorm Source Treatment Project aimed at restoring natural vegetation in croplands (Yin et al., 2018). These programs led to a reduction in croplands in the dry steppe and also a 15.5% reduction in the proportion of farmer households during 2000–2012, who had moved to cities for employment (Yin et al., 2018). Positive trends in the Ordos (Kubuqi desert and Mu Us Sandland) and Alashan (Badain Jarain desert) prefectures can also be explained by the growth of the Three Norths Shelterbelt program (also known as the Green Great Wall program) which was initiated in 1978 as windbreaks to hold back the eastward expansion of the Gobi desert (Cao et al., 2011; Tian et al., 2015). While these ecological restoration efforts by afforestation and dune stabilization have led to an increase in vegetation cover and AGB (Tian et al., 2015), there has been a concomitant decrease in ground water levels (Lu et al., 2018). This has been attributed to the high evapotranspiration of tree species (e.g. *Populus* spp) chosen for afforestation as compared to the native species of the desert steppe which include halophytic shrubs and herbaceous species (Cao et al., 2011; Lu et al., 2018).

4.3. Potential rangeland management application

Estimates of CC and AGB show a high degree of inter-annual variability and spatial heterogeneity. This suggests the need for rangeland management systems that are both flexible and adaptable to the dynamics of increasingly variable climate and timely access to forage. Owing to the high inter-annual variability, we chose to compare five year averages of July–August composites from 2000 to 2004 and 2012–2016 (Fig. 3, Fig. 4). Our estimated CC and AGB products have the potential to provide early warning of impending drought and reduced forage conditions (Fig. 5, Fig. S4) and can help enhance the capability of decision making tools such as the Mongolia Livestock Early Warning System (Kappas et al., 2015). One possible use of our CC and AGB deliverables are trend maps (Fig. 5), difference maps (Fig. S4) or standardized anomaly maps, calculated as seasonal composites subtracted from long term average (2000–2016) and divided by standard deviation for the same period. These anomaly maps highlight areas of above or below-average estimates of AGB. Along with ancillary information like rainfall prediction, herd location/size and water availability in watering holes, these trend and anomaly maps could provide livestock managers with options to reduce stocking rates in areas of strongly negative AGB and/or CC anomalies. The maps could also indicate forage deficits and re-direct herders to neighboring counties where there is a surplus of forage.

4.4. Cubist predictive models: Advantages and drawbacks

Our CC and AGB predictive models have advantages over linear regression models, which are mostly site-specific, limited by the amount of samples and the extent of in situ surveys. Rule-based models also have advantages over process-based models that are mostly dependent on site-level parametrizations, which are used as default over much broader range of vegetation types and climate regimes. This results in cascading error, especially when model simulations are over heterogeneous areas with large extent (Xiao et al., 2010; Wylie et al., 2016). In contrast, our predictive models were constrained by CC and AGB data from adequate sampling of herbaceous species across a wide range of steppe/biome types and precipitation regimes. Another major advantage of rule-based models is that they are effective in dealing with non-parametric data.

Our rule-based models were also very cost effective as they utilize a suite of publicly available, synoptic, geospatial data like MODIS with high spatiotemporal resolution as well as ancillary data sets like SRTM-derived DEMs. Furthermore, our predictive models consist of rule-based, multivariate regression models which are intuitive and easy to implement with less computational resources and complexity as compared to ecosystem models. The rule-based models uses input variables for model development (and consequently, mapping) only if their prediction utility is justified (Wylie et al., 2016). However, our rule-based models have some disadvantages when compared to process-based ecosystem models, as they do not account for underlying processes (e.g., photosynthesis, nitrogen cycling or deposition, and environmental stochasticity) (Zhang et al., 2012). These shortcomings might partly explain the differences between our estimates and process-based ecosystem model output (Xiao et al., 2010; Wylie et al., 2016). The difference in estimates could arise from the fact that rule-based models do not use factors that influence AGB, such as nitrogen availability and disturbance history, which can be explicitly modeled in process-based models.

5. Conclusions

We developed rule-based predictive models to estimate 8-day, spatially-explicit CC and AGB across the peak-growing season (July–August) on the Mongolian Plateau and environs. We synthesized multi-year, site-level observations of CC and AGB during the period 2006–2016 that represent the herbaceous vegetation of the meadow, typical and desert steppes. We then demonstrated the viability of using vegetation indices that were optimized for low canopy cover and water content and derived from MODIS NBAR surface reflectance to develop site-level predictive models for CC and AGB using non-parametric Cubist rule-based methods. These rule-based models were used to create spatially explicit, weekly, geospatial datasets of 500 m resolution to provide wall-to-wall coverage across the Mongolian Plateau. Predictive model estimates of CC and AGB were comparable to estimates of similar studies conducted in the area and are an improvement over standard MLR models. The maps and statistics presented illustrate inter-annual variability and trends in CC and AGB in the MP during the 2000–2016 period. Analysis of our ground sample data and scaled up estimates showed that they were significantly correlated with inter-annual climatic variability and anthropogenic drivers of change: population density, livestock density and distance to urban/built-up areas in provincial cities and towns/county headquarters. In addition to providing measures of carbon stock to the community, these predictive models offer decision makers and rangeland managers the ability to accurately monitor grassland dynamics, and control stocking rates in these remote and extensive grasslands. Our research study was based **on** extensive field sampling, used robust upscaling approaches, with high spatial resolution and temporal frequency and provides one of the

first set of gridded estimates of CC and AGB for the entire Mongolian Plateau. There is a need for further improvement and parameterization of regression tree predictive models by incorporating new observed data that is representative of steppe and cover types that were undersampled (i.e., desert and forest steppe) in both Mongolia and Inner Mongolia. There is a need for further investigation to identify the socioeconomic drivers of land use change in grassland ecosystems at finer spatial scales.

Acknowledgements

This study was supported by the "Dynamics of Coupled Natural and Human Systems (CNH)" Program of the NSF (#1313761), and the LCLUC program of NASA (NNX14AD85G). J. Xiao was supported by the National Science Foundation (NSF) through Macro Systems Biology (1638688) and NASA through the Carbon Cycle Science Program (NNX14AJ18G). We acknowledge the help of Ochirbat Batkhishig and Ganzorig Ulgichimeeg, Institute of Geography, Mongolian Academy of Sciences in organizing and supervising fieldwork. We also acknowledge the help of Jianye Xu, Ginger Allington and others for helping with field work, and Brad Peter for constructive suggestions regarding color blind sensitive maps. We thank the three anonymous reviewers for their constructive comments on the manuscript.

Appendix A. Supplementary data

Supplementary data to this article can be found online at https://doi.org/10.1016/j.rse.2018.05.002.

References

Ahlström, A., Raupach, M.R., Schurgers, G., Smith, B., Arneth, A., Jung, M., Reichstein, M., Canadell, J.G., Friedlingstein, P., Jain, A.K., Kato, E., Poulter, B., Sitch, S., Stocker, B.D., Viovy, N., Wang, Y.P., Wiltshire, A., Zaehle, S., Zeng, N., 2015. The dominant role of semi-arid ecosystems in the trend and variability of the land CO_2 sink. Science 348, 895.

Andersen, H.-E., McGaughey, R.J., Reutebuch, S.E., 2005. Estimating forest canopy fuel parameters using LIDAR data. Remote Sens. Environ. 94, 441–449.

Angerer, J.P. (Ed.), 2012. Gobi Forage Livestock Early Warning System. Food and Agriculture Organization, Rome, Italy.

Angerer, J., Han, G., Fujisaki, I., Havstad, K., 2008. Climate change and ecosystems of Asia with emphasis on inner Mongolia and Mongolia. Rangelands 30, 46–51.

Bai, Y., Han, X., Wu, J., Chen, Z., Li, L., 2004. Ecosystem stability and compensatory effects in the Inner Mongolia grassland. Nature 431, 181–184.

Bai, Y., Wu, J., Xing, Q., Pan, Q., Huang, J., Yang, D., Han, X., 2008. Primary production and rain use efficiency across a precipitation gradient on the Mongolia Plateau. Ecology 89, 2140–2153.

Blackard, J.A., Finco, M.V., Helmer, E.H., Holden, G.R., Hoppus, M.L., Jacobs, D.M., Lister, A.J., Moisen, G.G., Nelson, M.D., Riemann, R., Ruefenacht, B., Salajanu, D., Weyermann, D.L., Winterberger, K.C., Brandeis, T.J., Czaplewski, R.L., McRoberts, R.E., Patterson, P.L., Tymcio, R.P., 2008. Mapping U.S. forest biomass using nationwide forest inventory data and moderate resolution information. Remote Sens. Environ. 112, 1658–1677.

Bosilovich, M., Lucchesi, R., 2016. MERRA-2: File specification, GMAO Office Note No. 9, Version 1.1.

Breiman, L., 2001. Random forests. Mach. Learn. 45, 5–32.

Cao, S., Chen, L., Shankman, D., Wang, C., Wang, X., Zhang, H., 2011. Excessive reliance on afforestation in China's arid and semi-arid regions: lessons in ecological restoration. Earth Sci. Rev. 104, 240–245.

Chen, J., John, R., Zhang, Y., Shao, C., Brown, D.G., Batkhishig, O., Amarjargal, A., Ouyang, Z., Dong, G., Wang, D., Qi, J., 2015a. Divergences of two coupled human and natural systems on the Mongolian Plateau. Bioscience 65, 559–570.

Chen, J.Q., John, R., Shao, C.L., Fan, Y., Zhang, Y.Q., Amarjargal, A., Brown, D.G., Qi, J.G., Han, J.J., Lafortezza, R., Dong, G., 2015b. Policy shifts influence the functional changes of the CNH systems on the Mongolian plateau. Environ. Res. Lett. 10.

Chopping, M., Su, L., Rango, A., Martonchik, J.V., Peters, D.P.C., Laliberte, A., 2008. Remote sensing of woody shrub cover in desert grasslands using MISR with a geometric-optical canopy reflectance model. Remote Sens. Environ. 112, 19–34.

Eckert, S., Hüsler, F., Liniger, H., Hodel, E., 2015. Trend analysis of MODIS NDVI time series for detecting land degradation and regeneration in Mongolia. J. Arid Environ. 113, 16–28.

Fan, P., Chen, J., John, R., 2016. Urbanization and environmental change during the economic transition on the Mongolian Plateau: Hohhot and Ulaanbaatar. Environ. Res. 144, 96–112.

Feng, Z., Yang, Y., Zhang, Y., Zhang, P., Li, Y., 2005. Grain-for-green policy and its impacts on grain supply in West China. Land Use Policy 22, 301–312.

Fernández-Giménez, M.E., Allen-Diaz, B., 1999. Testing a non-equilibrium model of rangeland vegetation dynamics in Mongolia. J. Appl. Ecol. 36, 871–885.

Fernández-Giménez, M.E., Batkhishig, B., Batbuyan, B., 2012. Cross-boundary and cross-level dynamics increase vulnerability to severe winter disasters (dzud) in Mongolia. Glob. Environ. Chang. 22, 836–851.

Fernández-Giménez, M.E., Venable, N.H., Angerer, J., Fassnacht, S.R., Reid, R.S., Khishigbayar, J., 2017. Exploring linked ecological and cultural tipping points in Mongolia. Anthropocene 17, 46–69.

Ferner, J., Linstädter, A., Südekum, K.H., Schmidtlein, S., 2015. Spectral indicators of forage quality in West Africa's tropical savannas. Int. J. Appl. Earth Obs. Geoinf. 41, 99–106.

Gao, B.-c., 1996. NDWI—A normalized difference water index for remote sensing of vegetation liquid water from space. Remote Sens. Environ. 58, 257–266.

Gao, J.-X., Chen, Y.-M., Lü, S.-H., Feng, C.-Y., Chang, X.-L., Ye, S.-X., Liu, J.-D., 2012. A ground spectral model for estimating biomass at the peak of the growing season in Hulunbeier grassland, Inner Mongolia, China. Int. J. Remote Sens. 33, 4029–4043.

Giannico, V., Lafortezza, R., John, R., Sanesi, G., Pesola, L., Chen, J., 2016. Estimating stand volume and above-ground biomass of urban forests ssing LiDAR. Remote Sens. 8, 339.

Guan, K., Wood, E.F., Caylor, K.K., 2012. Multi-sensor derivation of regional vegetation fractional cover in Africa. Remote Sens. Environ. 124, 653–665.

Guerschman, J.P., Scarth, P.F., McVicar, T.R., Renzullo, L.J., Malthus, T.J., Stewart, J.B., Rickards, J.E., Trevithick, R., 2015. Assessing the effects of site heterogeneity and soil properties when unmixing photosynthetic vegetation, non-photosynthetic vegetation and bare soil fractions from Landsat and MODIS data. Remote Sens. Environ. 161, 12–26.

Halperin, J., LeMay, V., Coops, N., Verchot, L., Marshall, P., Lochhead, K., 2016. Canopy cover estimation in miombo woodlands of Zambia: comparison of Landsat 8 OLI versus RapidEye imagery using parametric, nonparametric, and semiparametric methods. Remote Sens. Environ. 179, 170–182.

Hilker, T., Natsagdorj, E., Waring, R.H., Lyapustin, A., Wang, Y., 2014. Satellite observed widespread decline in Mongolian grasslands largely due to overgrazing. Glob. Chang. Biol. 20, 418–428.

Huang, C., Townshend, J.R.G., 2003. A stepwise regression tree for nonlinear approximation: applications to estimating subpixel land cover. Int. J. Remote Sens. 24, 75–90.

Huete, A., Didan, K., Miura, T., Rodriguez, E.P., Gao, X., Ferreira, L.G., 2002. Overview of the radiometric and biophysical performance of the MODIS vegetation indices. Remote Sens. Environ. 83, 195–213.

Jackson, S.L., 2015. Dusty roads and disconnections: perceptions of dust from unpaved mining roads in Mongolia's south Gobi province. Geoforum 66, 94–105.

Jacques, D.C., Kergoat, L., Hiernaux, P., Mougin, E., Defourny, P., 2014. Monitoring dry vegetation masses in semi-arid areas with MODIS SWIR bands. Remote Sens. Environ. 153, 40–49.

Jiang, Z., Huete, A.R., Didan, K., Miura, T., 2008. Development of a two-band enhanced vegetation index without a blue band. Remote Sens. Environ. 112, 3833–3845.

John, R., Chen, J., Lu, N., Guo, K., Liang, C., Wei, Y., Noormets, A., Ma, K., Han, X., 2008. Predicting plant diversity based on remote sensing products in the semi-arid region of Inner Mongolia. Remote Sens. Environ. 112, 2018–2032.

John, R., Chen, J., Noormets, A., Xiao, X., Xu, J., Lu, N., Chen, S., 2013a. Modelling gross primary production in semi-arid Inner Mongolia using MODIS imagery and eddy covariance data. Int. J. Remote Sens. 34, 2829–2857.

John, R., Chen, J., Ou-Yang, Z.T., Xiao, J., Becker, R., Samanta, A., Ganguly, S., Yuan, W., Batkhishig, O., 2013b. Vegetation response to extreme climate events on the Mongolian Plateau from 2000 to 2010. Environ. Res. Lett. 8.

John, R., Chen, J., Kim, Y., Ou-yang, Z.-t., Xiao, J., Park, H., Shao, C., Zhang, Y., Amarjargal, A., Batkhshig, O., Qi, J., 2016. Differentiating anthropogenic modification and precipitation-driven change on vegetation productivity on the Mongolian Plateau. Landsc. Ecol. 31, 547–566.

Kang, M., Dai, C., Ji, W., Jiang, Y., Yuan, Z., Chen, H.Y.H., 2013. Biomass and its allocation in relation to temperature, precipitation, and soil nutrients in Inner Mongolia grasslands, China. PLoS One 8, e69561.

Kappas, M., Renchin, T., Munkhbayar, S., Vova, O., Degener, J., 2015. Review of long-term satellite data series on Mongolia for the study of land cover and land use. In: Karthe, D., Chalov, S., Kasimov, N., Kappas, M. (Eds.), Water and Environment in the Selenga-Baikal Basin. International Research Cooperation for an Ecoregion of Global Relevance, pp. 27–35 ibidem-Stuttgart.

Karnieli, A., Bayarjargal, Y., Bayasgalan, M., Mandakh, B., Dugarjav, C., Burgheimer, J., Khudulmur, S., Bazha, S.N., Gunin, P.D., 2013. Do vegetation indices provide a reliable indication of vegetation degradation? A case study in the Mongolian pastures. Int. J. Remote Sens. 34, 6243–6262.

Khishigbayar, J., Fernández-Giménez, M.E., Angerer, J.P., Reid, R.S., Chantsallkham, J., Baasandorj, Y., Zumberelmaa, D., 2015. Mongolian rangelands at a tipping point? Biomass and cover are stable but composition shifts and richness declines after 20 years of grazing and increasing temperatures. J. Arid Environ. 115, 100–112.

Kim, S., 2015. ppcor: an R package for a fast calculation to semi-partial correlation coefficients. In: Communications for statistical applications and methods. 22. pp. 665–674.

Kuhn, M., 2017. Package Caret. https://CRAN.R-project.org/package=caret.

Kuhn, M., Weston, S., Keefer, C., Coulter, N., Quinlan, R., 2017. Package 'Cubist'. pp. 13. https://CRAN.R-project.org/package=Cubist.

Lehnert, L.W., Meyer, H., Wang, Y., Miehe, G., Thies, B., Reudenbach, C., Bendix, J., 2015. Retrieval of grassland plant coverage on the Tibetan Plateau based on a multi-scale, multi-sensor and multi-method approach. Remote Sens. Environ. 164, 197–207.

Li, F., Chen, W., Zeng, Y., Zhao, Q., Wu, B., 2014. Improving estimates of grassland

fractional vegetation cover based on a pixel dichotomy model: a case study in Inner Mongolia, China. Remote Sens. 6.
Liang, T., Yang, S., Feng, Q., Liu, B., Zhang, R., Huang, X., Xie, H., 2016. Multi-factor modeling of above-ground biomass in alpine grassland: a case study in the Three-River headwaters region, China. Remote Sens. Environ. 186, 164–172.
Liu, G., Xie, X., Ye, D., Ye, X., Tuvshintogtokh, I., Mandakh, B., Huang, Z., Dong, M., 2013. Plant functional diversity and species diversity in the Mongolian steppe. PLoS One 8, e77565.
Lobser, S.E., Cohen, W.B., 2007. MODIS tasselled cap: land cover characteristics expressed through transformed MODIS data. Int. J. Remote Sens. 28, 5079–5101.
Lu, Y., Zhuang, Q., Zhou, G., Sirin, A., Melillo, J., Kicklighter, D., 2009. Possible decline of the carbon sink in the Mongolian Plateau during the 21st century. Environ. Res. Lett. 4, 045023.
Lu, C., Zhao, T., Shi, X., Cao, S., 2018. Ecological restoration by afforestation may increase groundwater depth and create potentially large ecological and water opportunity costs in arid and semiarid China. J. Clean. Prod. 176, 1213–1222.
Ma, W., Fang, J., Yang, Y., Mohammat, A., 2010. Biomass carbon stocks and their changes in northern China's grasslands during 1982–2006. Sci. China Life Sci. 53, 841–850.
Marsett, R.C., Qi, J., Heilman, P., Biedenbender, S.H., Watson, M.C., Amer, S., Weltz, M., Goodrich, D., Marsett, R., 2006. Remote sensing for grassland management in the arid southwest. Rangel. Ecol. Manag. 59, 530–540.
McIntyre, N., Bulovic, N., Cane, I., McKenna, P., 2016. A multi-disciplinary approach to understanding the impacts of mines on traditional uses of water in Northern Mongolia. Sci. Total Environ. 557-558, 404–414.
Nandintsetseg, B., Greene, J.S., Goulden, C.E., 2007. Trends in extreme daily precipitation and temperature near lake Hövsgöl, Mongolia. Int. J. Climatol. 27, 341–347.
NASA-JPL, 2013. NASA Shuttle Radar Topography Mission Global 1 Arc Second. NASA LP DAAC.
Park, H., Fan, P., John, R., Chen, J., 2017. Urbanization on the Mongolian Plateau after economic reform: changes and causes. Appl. Geogr. 86, 118–127.
Poulter, B., Frank, D., Ciais, P., Myneni, R.B., Andela, N., Bi, J., Broquet, G., Canadell, J.G., Chevallier, F., Liu, Y.Y., Running, S.W., Sitch, S., van der Werf, G.R., 2014. Contribution of semi-arid ecosystems to interannual variability of the global carbon cycle. Nature 509, 600–603.
Qi, J., Marsett, R., Heilman, P., Bieden-bender, S., Moran, S., Goodrich, D., Weltz, M., 2002. RANGES improves satellite-based information and land cover assessments in southwest United States. In: Eos. 83. Transactions American Geophysical Union, pp. 601–606.
Qi, J., Xin, X., John, R., Groisman, P., Chen, J., 2017. Understanding livestock production and sustainability of grassland ecosystems in the Asian Dryland Belt. Ecol. Process. 6, 22.
Quinlan, R., 1993. C4.5: Programs for Machine Learning. Morgan Kaufmann Publishers Inc., San Francisco, CA.
Rao, M.P., Davi, N.K., D'Arrigo, R.D., Skees, J., Baatarbileg, N., Leland, C., Lyon, B., Wang, S., Byambasuren, O., 2015. Dzuds, droughts, and livestock mortality in Mongolia. Environ. Res. Lett. 10, 074012.
Rasmussen, M.S., James, R., Adiyasuren, T., Khishigsuren, P., Naranchimeg, B., Gankhuyag, R., Baasanjargal, B., 1999. Supporting Mongolian pastoralists by using GIS to identify grazing limitations and opportunities from livestock census and remote sensing data. GeoJournal 47, 563–571.
Reid, R.S., Fernández-Giménez, M.E., Galvin, K.A., 2014. Dynamics and resilience of rangelands and pastoral peoples around the globe. Annu. Rev. Environ. Resour. 39, 217–242.
Reynolds, J.F., Smith, D.M.S., Lambin, E.F., Turner, B.L., Mortimore, M., Batterbury, S.P.J., Downing, T.E., Dowlatabadi, H., Fernández, R.J., Herrick, J.E., Huber-Sannwald, E., Jiang, H., Leemans, R., Lynam, T., Maestre, F.T., Ayarza, M., Walker, B., 2007. Global desertification: building a science for dryland development. Science 316, 847–851.
Rienecker, M.M., Suarez, M.J., Gelaro, R., Todling, R., Bacmeister, J., Liu, E., Bosilovich, M.G., Schubert, S.D., Takacs, L., Kim, G.-K., Bloom, S., Chen, J., Collins, D., Conaty, A., da Silva, A., Gu, W., Joiner, J., Koster, R.D., Lucchesi, R., Molod, A., Owens, T., Pawson, S., Pegion, P., Redder, C.R., Reichle, R., Robertson, F.R., Ruddick, A.G., Sienkiewicz, M., Woollen, J., 2011. MERRA: NASA's modern-era retrospective analysis for research and applications. J. Clim. 24, 3624–3648.
Schaaf, C., 2015. MCD43A4 MODIS/Terra + Aqua BRDF/Albedo Nadir BRDF Adjusted RefDaily L3 Global – 500m V006. NASA EOSDIS Land Processes DAAChttp://dx.doi.org/10.5067/MODIS/MCD43A4.006.
Schaaf, C.B., Gao, F., Strahler, A.H., Lucht, W., Li, X., Tsang, T., Strugnell, N.C., Zhang, X., Jin, Y., Muller, J.-P., Lewis, P., Barnsley, M., Hobson, P., Disney, M., Roberts, G., Dunderdale, M., Doll, C., d'Entremont, R.P., Hu, B., Liang, S., Privette, J.L., Roy, D., 2002. First operational BRDF, albedo nadir reflectance products from MODIS. Remote Sens. Environ. 83, 135–148.
Sen, P.K., 1968. Estimates of the regression coefficient based on Kendall's Tau. J. Am. Stat. Assoc. 63, 1379–1389.
Shao, C., Chen, J., Li, L., 2013. Grazing alters the biophysical regulation of carbon fluxes in a desert steppe. Environ. Res. Lett. 8, 025012.
Tian, H., Cao, C., Chen, W., Bao, S., Yang, B., Myneni, R.B., 2015. Response of vegetation activity dynamic to climatic change and ecological restoration programs in Inner Mongolia from 2000 to 2012. Ecol. Eng. 82, 276–289.
Tucker, C.J., Sellers, P.J., 1986. Satellite remote sensing of primary production. Int. J. Remote Sens. 7, 1395–1416.
Uchida, E., Xu, J., Rozelle, S., 2005. Grain for green: cost-effectiveness and sustainability of China's conservation set-aside program. Land Econ. 81, 247–264.
Walton, J.T., 2008. Subpixel urban land cover estimation. Photogramm. Eng. Remote. Sens. 74, 1213–1222.
Wang, J., Brown, D., Chen, J., 2013. Drivers of the dynamics in net primary productivity across ecological zones on the Mongolian Plateau. Landsc. Ecol. 28, 725–739.
Wesche, K., Ronnenberg, K., Retzer, V., Miehe, G., 2010. Effects of large herbivore exclusion on southern Mongolian desert steppes. Acta Oecol. 36, 234–241.
Wesche, K., Ambarlı, D., Kamp, J., Török, P., Treiber, J., Dengler, J., 2016. The Palaearctic steppe biome: a new synthesis. Biodivers. Conserv. 25, 2197–2231.
Wylie, B., Howard, D., Dahal, D., Gilmanov, T., Ji, L., Zhang, L., Smith, K., 2016. Grassland and cropland net ecosystem production of the U.S. Great Plains: regression tree model development and comparative analysis. Remote Sens. 8.
Xiao, X., Boles, S., Liu, J., Zhuang, D., Liu, M., 2002. Characterization of forest types in Northeastern China, using multi-temporal SPOT-4 VEGETATION sensor data. Remote Sens. Environ. 82, 335–348.
Xiao, J., Zhuang, Q., Baldocchi, D.D., Law, B.E., Richardson, A.D., Chen, J., Oren, R., Starr, G., Noormets, A., Ma, S., Verma, S.B., Wharton, S., Wofsy, S.C., Bolstad, P.V., Burns, S.P., Cook, D.R., Curtis, P.S., Drake, B.G., Falk, M., Fischer, M.L., Foster, D.R., Gu, L., Hadley, J.L., Hollinger, D.Y., Katul, G.G., Litvak, M., Martin, T.A., Matamala, R., McNulty, S., Meyers, T.P., Monson, R.K., Munger, J.W., Oechel, W.C., Paw, U.K.T., Schmid, H.P., Scott, R.L., Sun, G., Suyker, A.E., Torn, M.S., 2008. Estimation of net ecosystem carbon exchange for the conterminous United States by combining MODIS and AmeriFlux data. Agric. For. Meteorol. 148, 1827–1847.
Xiao, J., Zhuang, Q., Law, B.E., Chen, J., Baldocchi, D.D., Cook, D.R., Oren, R., Richardson, A.D., Wharton, S., Ma, S., Martin, T.A., Verma, S.B., Suyker, A.E., Scott, R.L., Monson, R.K., Litvak, M., Hollinger, D.Y., Sun, G., Davis, K.J., Bolstad, P.V., Burns, S.P., Curtis, P.S., Drake, B.G., Falk, M., Fischer, M.L., Foster, D.R., Gu, L., Hadley, J.L., Katul, G.G., Matamala, R., McNulty, S., Meyers, T.P., Munger, J.W., Noormets, A., Oechel, W.C., Paw, U.K.T., Schmid, H.P., Starr, G., Torn, M.S., Wofsy, S.C., 2010. A continuous measure of gross primary production for the conterminous United States derived from MODIS and AmeriFlux data. Remote Sens. Environ. 114, 576–591.
Xie, Y., Sha, Z., Yu, M., Bai, Y., Zhang, L., 2009. A comparison of two models with Landsat data for estimating above ground grassland biomass in Inner Mongolia, China. Ecol. Model. 220, 1810–1818.
Yin, H., Pflugmacher, D., Li, A., Li, Z., Hostert, P., 2018. Land use and land cover change in Inner Mongolia - understanding the effects of China's re-vegetation programs. Remote Sens. Environ. 204, 918–930.
Yu, F., Price, K.P., Ellis, J., Shi, P., 2003. Response of seasonal vegetation development to climatic variations in eastern central Asia. Remote Sens. Environ. 87, 42–54.
Zhang, F., Chen, J.M., Chen, J., Gough, C.M., Martin, T.A., Dragoni, D., 2012. Evaluating spatial and temporal patterns of MODIS GPP over the conterminous U.S. against flux measurements and a process model. Remote Sens. Environ. 124, 717–729.
Zhang, L., Guo, H., Jia, G., Wylie, B., Gilmanov, T., Howard, D., Ji, L., Xiao, J., Li, J., Yuan, W., Zhao, T., Chen, S., Zhou, G., Kato, T., 2014. Net ecosystem productivity of temperate grasslands in northern China: an upscaling study. Agric. For. Meteorol. 184, 71–81.
Zhang, C., Lu, D., Chen, X., Zhang, Y., Maisupova, B., Tao, Y., 2016. The spatiotemporal patterns of vegetation coverage and biomass of the temperate deserts in Central Asia and their relationships with climate controls. Remote Sens. Environ. 175, 271–281.
Zhao, F., Xu, B., Yang, X., Jin, Y., Li, J., Xia, L., Chen, S., Ma, H., 2014. Remote sensing estimates of grassland aboveground biomass based on MODIS net primary productivity (NPP): a case study in the Xilingol grassland of northern China. Remote Sens. 6.